*Geophys. J. Int.* (1990) **101,** 739–750 *and microfiche* GJI 101/1

# Wave propagation in anisotropic linear viscoelastic media: theory and simulated wavefields

J. M. Carcione

*Geophysical Institute, Hamburg University, Bundesstrasse* 55, 2000 *Hamburg* 13, *FRG, and Osservatorio Geofisico Sperimentale, PO Box* 2011, 34016 *Trieste, Italy*

Accepted 1990 January 11. Received 1990 January 11; in original form 1988 October 10

## SUMMARY

The anisotropic linear viscoelastic rheological relation constitutes a suitable model for describing the variety of phenomena which occur in seismic wavefields. This rheology, known also as Boltzmann's superposition principle, expresses the stress as a time convolution of a fourth rank tensorial relaxation function with the strain tensor.

The first problem is to establish the time dependence of the relaxation tensor in a general and consistent way. Two kernels based on the general standard linear solid are identified with the mean stress and with the deviatoric components of the stress tensor in a given coordinate system, respectively. Additional conditions are that in the elastic limit the relaxation matrix must give the elasticity matrix, and in the isotropic limit the relaxation matrix must approach the isotropic–viscoelastic matrix. The resulting rheological relation provides the framework for incorporating anelasticity in time-marching methods for computing synthetic seismograms. Through a plane wave analysis of the anisotropic–viscoelastic medium, the phase, group and energy velocities are calculated in function of the complex velocity, showing that those velocities are in general different from each other. For instance, the energy velocity which represents the wave surface, is different from the group velocity unlike in the anisotropic–elastic case. The group velocity loses its physical meaning at the cusps where singularities appear. Each frequency component of the wavefield has a different non-spherical wavefront. Moreover, the quality factors for the different propagating modes are not isotropic. Examples of these physical quantities are shown for transversely isotropic–viscoelastic clayshale and sandstone.

As in the isotropic–viscoelastic case, Boltzmann's superposition principle is implemented in the equation of motion by defining memory variables which circumvent the convolutional relation between stress and strain. The numerical problem is solved by using a new time integration technique specially designed to deal with wave propagation in linear viscoelastic media. As a first application snapshots and synthetic seismograms are computed for 2-D transversely isotropic–viscoelastic clayshale and sandstone which show substantial differences in amplitude, waveform and arrival time with the results given by the isotropic and elastic rheologies.

**Key words:** anisotropy, attenuation, dispersion, modelling, viscoelasticity.

## INTRODUCTION

The following abbreviations are used for simplicity: IE: isotropic–elastic, IV: isotropic–viscoelastic, TIE: transversely isotropic–elastic, AE: anisotropic–elastic, TIV: transversely isotropic–viscoelastic, and AV: anisotropic–viscoelastic.

With the improvement in data quality and the use of new exploration techniques, the correct description of the seismic wavefield has become more important. This task has become feasible with the development of new algorithms for solving the governing equation of motion, and the availability of better computational facilities. An appropriate theory for describing wave propagation in the Earth should include all the phenomena which can be detected and measured in real seismic data. Of importance to earthquake seismologists and exploration geophysicists is the following approximate chronological order for the introduction of the different rheologies in seismic modelling.

(a) A first approximation to model the compressional wavefield or $P$-wave by assuming the acoustic rheology. In general, the commercial processing software for petroleum geophysics is based on this approximation.

(b) The IE rheology to replace the acoustic assumption (see for instance Alekseev & Mikhailenko, 1980; Kosloff, Reshef & Loewenthal 1984; Virieux 1986; Kummer, Behle & Dorau 1987), which gives the distinction between the compressional and the shear wavefields, and the conversion from one mode to the other.

(c) The incorporation of attenuation into the acoustic rheology, giving the viscoacoustic stress–strain relation (Krebes & Hron 1980; Day & Minster 1984; Emmerich & Korn 1987; Carcione, Kosloff & Kosloff 1988a, b). This rheology explains the attenuation and dispersion of the dilatational wavefield.

(d) The IV rheology (see for instance Mikhailenko 1985; Carcione *et al.* 1988c), which in many aspects describes new effects compared to the purely elastic case (Buchen 1971; Borcherdt & Wennerberg 1985); for instance, the existence of inhomogeneous waves (not the interface waves of elastic media) makes it necessary to satisfy the boundary conditions on anelastic interfaces. For these waves the propagation direction does not coincide with the attenuation direction, particle motions are elliptical, and critical angles do not exist in general but only under particular circumstances. In general, a wave travelling through a layered media has an angular dependence of attenuation and dispersion, where the more oblique direction has more energy dissipation and lower velocity.

(e) The AE rheology (see for instance White 1982; Booth & Crampin 1983; Martynov & Mikhailenko 1984; Fryer & Frazer 1987; Gajewski & Pšenčík 1988; Carcione *et al.* 1988d), which introduces new phenomena, for instance shear wave splitting (Crampin 1985). The most important consequences of this rheology are that in general, the wavefield is not pure longitudinal or pure transverse, and therefore there is no simple relation between the propagation direction and the direction of particle displacement; wavefronts are not spherical; the direction of energy flux (rays) does not coincide with the wavenumber direction. A secondary effect, not detected yet in seismic data, are the cusps present in one of the shear modes.

A further and natural step for obtaining a realistic description, i.e., the inclusion in wave propagation of all the phenomena mentioned before, is the implementation of the linear AV constitutive relation in the equation of motion. The linear assumption for the dissipation mechanisms is justified by experimental results found for seismic strains and upper crustal conditions (Jones 1986). Anelasticity is due to a rather large number of physical mechanisms depending on the frequency band (Biot 1962; O'Connell & Budiansky 1977; Murphy, Winkler & Kleinberg 1986; etc.). A general way to account for all these mechanisms is to use a phenomenological model which can fit any particular theory and also real data. On the other hand, anisotropy is well described by the generalized Hooke's law, i.e., by 21 independent elastic constants in a 3-D medium, and six elastic constants in a 2-D medium.

The most general rheology under these circumstances is the isothermal AV constitutive relation (Christensen 1982), in which the stress and the strain tensors are related by a time-dependent relaxation tensor through a convolution integral. The first problem is to establish the time dependence of the relaxation tensor in a general and consistent way. The kernel represented by the general standard linear solid is the basis for constructing this time dependence. A general viscoelastic solid can be obtained by considering several standard linear elements in parallel or in series. It is important, particularly in exploration seismology, that the material rheology gives causal behaviour and approximately a constant $Q$ factor in the exploration seismic band, although the kernel can fit any general $Q$ function no matter what the frequency range. The process of wave propagation in porous media can be approximated by a linear viscoelastic solid when wave propagating modes are considered. It was showed by Geertsma & Smit (1961) that to describe $P$-wave propagation in a Biot medium one standard linear element is sufficient.

Two kernels or relaxation functions are identified, one of them with the mean stress which is invariant under transformations of the coordinate system, and the other with the deviatoric components of the stress tensor in a given coordinate system. In this way it is possible to establish the anelastic characteristics of the three propagating modes, the quasi-longitudinal and the two shear modes. Two additional conditions are imposed: (i) in the AE limit the relaxation matrix must approach the elasticity matrix, and (ii) in the IV limit the relaxation matrix must give the isotropic–viscoelastic matrix defined in Carcione *et al.* (1988c). The resulting constitutive relation, although not unique, represents a general and consistent way to introduce anelasticity into the generalized Hooke's law. The preceding conditions establish the time dependence of the relaxation matrix components on physical grounds, and maintain the simplicity of the isotropic case where only two kernels are necessary to define the anelastic properties. As in the IV wave propagation problem, Boltzmann's superposition principle is implemented in the equation of motion by defining memory variables which circumvent the convolutional relation between stress and strain. For instance, the solution of the 2-D problem implies the introduction of three memory variables, one for each dilatational relaxation mechanism and two for each shear relaxation mechanism.

This work concentrates on the issue of wave propagation in the Earth. However, the subject of wave propagation in AV media has practical a value in many other fields, for instance applied mechanics and physics of materials (see for instance Lamb & Richter 1966; Szilard 1982). The first section establishes the constitutive relation. Then, the equation of motion for a general inhomogeneous AV medium is derived. Finally, examples of wave propagation in 2-D homogeneous and inhomogeneous TIV real earth materials are considered, with comparisons to the more simple rheologies. The microfiche contains the following material: first a detailed derivation of the constitutive relation; then a plane wave analysis establishes the energy balance equation and the phase, group and energy velocities of the AV medium, with 3-D examples for TIV earth media; finally, the derivation of the equation of motion for 2-D TIV media with simulated wavefields in sandstone.

## CONSTITUTIVE RELATION

The stress–strain relation is simplified by introducing a shortened matrix notation where pairs of subscripts are replaced by a single number according to the following correspondences: $(11)\rightarrow 1$, $(22)\rightarrow 2$, $(33)\rightarrow 3$, $(23)=(32)\rightarrow 4$, $(13)=(31)\rightarrow 5$, $(12)=(21)\rightarrow 6$. The convention will be to denote abbreviated subscripts by upper case letters and full subscripts by lower case letters.

A response of the earth is described by Boltzmann's superposition principle which can be expressed as (see Appendix A in microfiche):

$$\mathbf{T}(\mathbf{x}, t) = \Psi(\mathbf{x}, t) * \dot{\mathbf{S}}(\mathbf{x}, t), \tag{1}$$

with

$$\mathbf{T}^{\mathrm{T}} = (T_1, T_2, T_3, T_4, T_5, T_6) = (\sigma_{xx}, \sigma_{yy}, \sigma_{zz}, \sigma_{yz}, \sigma_{xz}, \sigma_{xy}) \tag{2}$$

the stress vector, where $\sigma_{ij}$, $i, j = 1, \ldots, 3$ are the stress components, and

$$\mathbf{S}^{\mathrm{T}} = (S_1, S_2, S_3, S_4, S_5, S_6) = (\varepsilon_{xx}, \varepsilon_{yy}, \varepsilon_{zz}, 2\varepsilon_{yz}, 2\varepsilon_{xz}, 2\varepsilon_{xy}) \tag{3}$$

the strain vector, where $\varepsilon_{ij}$, $i, j = 1, \ldots, 3$ are the strain components; $\Psi$ is the symmetric relaxation matrix with components $\psi_{IJ}$, $I, J = 1, \ldots, 6$; $t$ is the time variable, $\mathbf{x}$ is the position vector, the symbol '$*$' indicates time convolution, and a dot above a variable implies time differentiation. Vectors are written as columns with the superscript 'T' denoting the transpose.

Equation (1) can be written in components as

$$T_I = \psi_{IJ} * \dot{S}_J, \qquad I, J = 1, \ldots, 6 \tag{4}$$

where the Einstein convention for repeated indices is used. In Appendix A, the following stress–strain relation is established:

$$T_I = \psi_{IJ} * \dot{S}_J = \{[A_{IJ} + A_{IJ}^{(\nu)}\chi_\nu(t)]H(t)\} * \dot{S}_J, \tag{5}$$

where $\chi_\nu$, $\nu = 1, 2$ are time-dependent functions, and $A_{IJ}$ and $A_{IJ}^{(\nu)}$ are space-dependent functions. The conditions on the relaxation components are that the trace of the stress tensor should depend on the time variable only through the kernel $\chi_1$, and the deviatoric components of the stress tensor in a given system $S$ should depend on the time variable only through the kernel $\chi_2$. The trace of the stress tensor is invariant under transformation of the coordinate system. This fact assures that the mean tension (one third of the trace) is related only to the function $\chi_1$ in any system. Hence, this function describes dilatational deformations. The deviatoric components are not invariants but a cube of material orientated in the direction of the axes of the system $S$ will be subjected to shear deformations exclusively related to the function $\chi_2$. In general, experimental values of the attenuation coefficient and the quality factor are given with respect to material axes (Lamb & Richter 1966). With this condition for instance, the value of the shear quality factors in the symmetry axis of a TIV medium can be established. Additional conditions are that in the AE limit the relaxation matrix must give the elasticity matrix, and that in the IV limit the relaxation matrix must give the isotropic-viscoelastic matrix (Carcione *et al.* 1988c). In Appendix A an appropiate 3-D AV relaxation matrix is obtained which has the form

$$\Psi = \begin{pmatrix} \psi_{11} & \psi_{12} & \psi_{13} & c_{14} & c_{15} & c_{16} \\ & \psi_{22} & \psi_{23} & c_{24} & c_{25} & c_{26} \\ & & \psi_{33} & c_{34} & c_{35} & c_{36} \\ & & & c_{44}\chi_2 & c_{45}\chi_2 & c_{46}\chi_2 \\ & & & & c_{55}\chi_2 & c_{56}\chi_2 \\ & & & & & c_{66}\chi_2 \end{pmatrix} H \tag{6}$$

with

$$\psi_{11} = c_{11} - D + (D - \tfrac{4}{3}G)\chi_1 + \tfrac{4}{3}G\chi_2, \tag{7a}$$

$$\psi_{12} = c_{12} - D + 2G + (D - \tfrac{4}{3}G)\chi_1 - \tfrac{2}{3}G\chi_2, \tag{7b}$$

$$\psi_{13} = c_{13} - D + 2G + (D - \tfrac{4}{3}G)\chi_1 - \tfrac{2}{3}G\chi_2, \tag{7c}$$

$$\psi_{22} = c_{22} - D + (D - \tfrac{4}{3}G)\chi_1 + \tfrac{4}{3}G\chi_2, \tag{7d}$$

$$\psi_{23} = c_{23} - D + 2G + (D - \tfrac{4}{3}G)\chi_1 - \tfrac{2}{3}G\chi_2, \tag{7e}$$

and

$$\psi_{33} = c_{33} - D + (D - \tfrac{4}{3}G)\chi_1 + \tfrac{4}{3}G\chi_2, \tag{7f}$$

where $H(t)$ is the Heaviside function,

$$D = (c_{11} + c_{22} + c_{33})/3 \tag{7g}$$

and

$$G = (c_{44} + c_{55} + c_{66})/3. \tag{7h}$$

The quantities $c_{IJ}$, $I, J = 1, 6$ represent space-dependent elasticities, and

$$\chi_\nu = \left[1 - \sum_{l=1}^{L_\nu}\left(1 - \frac{\tau_{el}^{(\nu)}}{\tau_{\sigma l}^{(\nu)}}\right)\mathrm{e}^{-t/\tau_{\sigma l}^{(\nu)}}\right], \qquad \nu = 1, 2 \tag{8}$$

are relaxation functions which correspond to states of quasi-dilatation ($\nu = 1$), and quasi-shear ($\nu = 2$), respectively. The quantities $\tau_{el}^{(\nu)}(\mathbf{x})$ and $\tau_{\sigma l}^{(\nu)}(\mathbf{x})$ denote material relaxation times for $l$th mechanism, and $L_\nu$ is the number of relaxation mechanisms. Although the kernels $\chi_\nu$ are based on the standard linear solid any appropriate kernel can also be used, for instance the generalized Maxwell body given by Emmerich & Korn (1987).

An example of a 2-D relaxation matrix is

$$\Psi = \begin{pmatrix} \psi_{11} & \psi_{12} & c_{15} \\ & \psi_{22} & c_{35} \\ & & c_{55}\chi_2 \end{pmatrix} H, \tag{9}$$

with

$$\psi_{11} = c_{11} - D + (D - c_{55})\chi_1 + c_{55}\chi_2, \tag{10a}$$

$$\psi_{12} = c_{13} + 2c_{55} - D + (D - c_{55})\chi_1 - c_{55}\chi_2, \tag{10b}$$

$$\psi_{22} = c_{33} - D + (D - c_{55})\chi_1 + c_{55}\chi_2, \tag{10c}$$

and

$$D = (c_{11} + c_{33})/2, \tag{10d}$$

where the $(x, z)$-plane has been considered. The elastic limit is obtained when $\chi_v \to 1$, $v = 1, 2$, which can be verified easily in equations (6) and (9).

Uniform plane waves provide a very useful tool for analysing characteristics of wave propagation. In Appendix B (microfiche) a plane wave analysis of an AV medium is performed. First the energy balance equation or complex Poynting's theorem is established. Then, the Christoffel equation and dispersion relation. Finally, the complex and physical velocities of the three modes are obtained together with the quality factors for homogeneous waves. Physical velocities mean the phase velocity or wavefront velocity along the propagation direction, the group velocity or velocity of the modulation envelope of the wave, and the energy velocity which has the direction of the Poynting vector, and its representation defines the wave surface. As a consequence, the relations among the different physical velocities and quality factors for the various rheologies are summarized. The examples show the wave propagation characteristics of a TIV clayshale and a TIV sandstone. The Appendix contains also a verification of the physical realizability conditions of the relaxation matrix.

## EQUATION OF MOTION

The equation of motion for a 3-D anisotropic linear anelastic medium is

$$\boldsymbol{\nabla} \cdot \mathbf{T} = \rho \ddot{\mathbf{u}} + \mathbf{f}, \tag{11}$$

or in components

$$\nabla_{iJ} T_J = \rho \ddot{u}_i + f_i, \tag{12}$$

where $\mathbf{u}(\mathbf{x}, t)$ is the displacement vector, $\mathbf{f}(\mathbf{x}, t)$ is the body forces vector, $\rho(\mathbf{x})$ is the density, and '$\boldsymbol{\nabla}\cdot$' is a divergence operator defined by

$$\boldsymbol{\nabla}\cdot \to \nabla_{iJ} = \begin{pmatrix} \partial/\partial x & 0 & 0 & 0 & \partial/\partial z & \partial/\partial y \\ 0 & \partial/\partial y & 0 & \partial/\partial z & 0 & \partial/\partial x \\ 0 & 0 & \partial/\partial z & \partial/\partial y & \partial/\partial x & 0 \end{pmatrix}. \tag{13}$$

As in the IV wave propagation problem (Carcione *et al.* 1988c), implementation of the rheological relation (5) is not straightforward because of the presence of convolutional kernels. Consequently, in this section the constitutive equation is reformulated to yield a more convenient description. Let the relaxation matrix be known in system $S'$, and the problem solved in system $S$. Therefore, the relaxation components transform as

$$\psi_{IJ} = t_{IL} t_{JK} \psi'_{LK}, \tag{14}$$

where $\Psi'$ is the relaxation matrix in system $S'$, and $\mathbf{T}$ is a $6 \times 6$ rotation with components $t_{IJ}$ (see Appendix C in microfiche). These components can be space dependent. Combining equations (5) and (14) and using properties of the convolution gives

$$T_I = t_{IL} t_{JK} \left[ A_{LK} S_J + A_{LK}^{(v)} \frac{d}{dt} (\chi_v H) * S_J \right] \tag{15}$$

where the primes in the relaxation components are omitted for clarity. Equation (15) is equivalent to

$$T_I = t_{IL} t_{JK} \{ [A_{LK} + A_{LK}^{(v)} \chi_v(0)] S_J + A_{LK}^{(v)} \dot{\chi}_v * S_J \}, \tag{16}$$

after the integration of the resulting delta function. Performing the time derivative [see equation (8)], yields

$$T_I = t_{IL} t_{JK} \left\{ [(A_{LK} + A_{LK}^{(v)} M_{uv}] S_J + A_{LK}^{(v)} \sum_{l=1}^{L_v} \varphi_{vl} * S_J \right\}, \tag{17}$$

where

$$\varphi_{vl} = \frac{1}{\tau_{\sigma l}^{(v)}} \left( 1 - \frac{\tau_{\epsilon l}^{(v)}}{\tau_{\sigma l}^{(v)}} \right) e^{-t/\tau_{\sigma l}^{(v)}}, \qquad l = l, \ldots, L_v \tag{18}$$

is called the response function of the $l$th relaxation mechanism, and $M_{uv} \equiv \chi_v(0)$ is the unrelaxed modulus. The function $\varphi_{vl}$ obeys the following differential equation:

$$\dot{\varphi}_{vl}(t) = -\varphi_{vl}(t)/\tau_{\sigma l}^{(v)}. \tag{19}$$

Now the following memory variables are defined:

$$e_{Jl}^{(v)} = \varphi_{vl} * S_J, \; v = 1, 2, \; J = 1, \ldots, 6, \; l = 1, \ldots, L_v. \tag{20}$$

Replacing these quantities in (17) yields

$$T_I = t_{IL} t_{JK} \left\{ [A_{LK} + A_{LK}^{(v)} M_{uv}] S_J + A_{LK}^{(v)} \sum_{l=1}^{L_v} e_{JL}^{(v)} \right\}. \tag{21}$$

Time defferentiating equation (20) gives

$$\dot{e}_{Jl}^{(v)} = S_J \varphi_{vl}(0) - e_{Jl}^{(v)}/\tau_{\sigma l}^{(v)}, \qquad l = 1, \ldots, L_v, \tag{22}$$

where equation (19) has been used. Equation (21) and (22) together with the equation of motion (12) fully describe the response of the AV medium, and will be the basis for the numerical solution algorithm. After substitution of (21) in (12), and with equations (22) and the strain–displacement relations, a first-order differential equation in time is obtained:

$$\dot{\mathbf{U}} = \mathbf{M}\mathbf{U} + \mathbf{F}, \tag{23}$$

where $\mathbf{U}$ is the unknown variable vector formally given by

$$\mathbf{U}^{\mathrm{T}} = (\mathbf{u}, \dot{\mathbf{u}}, e_{Jl}^{(v)}), \tag{24}$$

$\mathbf{F}$ is the body force vector represented by

$$\mathbf{F}^{\mathrm{T}} = (\mathbf{0}, \mathbf{f}/\rho, \mathbf{0}), \tag{25}$$

and $\mathbf{M}$ is an operator matrix which contains the spatial derivative operators and all the material parameters defining the medium. In the next section this operator is given explicitly for the 2-D case. The number of memory variables depends on the particular choice of the relaxation matrix, but in principle they are reduced in virtue of the restrictions imposed on the relaxation components. The rotation type also restricts the number of variables. It can be seen that when $\mathbf{T}$ is the identity matrix, the number of variables reduce to a minimum. An alternative method to equation (14) is to apply the transformation to the elasticity matrix $\mathbf{C}$ (whose components are $c_{IJ}$, $I, J = 1, \ldots, 6$) and then introduce the anelasticity. Of course these two different approaches do not give the same results, but the latter case requires a minimum of variables. In the next section an example of 2-D wave propagation is considered, where the problem can be treated with three variables for each relaxation mechanism.

The differential equation (23) represents the equation of motion for the AV medium which correctly describes anisotropic and anelastic effects in wave propagation within the framework of the linear response theory.

The solution of (23) subject to the initial condition $\mathbf{U}(t=0)=\mathbf{U}_0$ is formally given by

$$\mathbf{U}=e^{t\mathbf{M}}\mathbf{U}_0+\int_0^t e^{\tau\mathbf{M}}\mathbf{F}(t-\tau)\,d\tau. \tag{26}$$

In equation (26), $e^{t\mathbf{M}}$ is called the evolution operator of the system. Most frequently an explicit or implicit finite difference scheme is used to march the solution in time in the AE and IV wave propagation problems. This technique is based on a Taylor expansion of the evolution operator. This work uses a new time integration method which is specially designed to deal with wave propagation in linear AV media. The new approach is based on a polynomial interpolation of the exponential function in the complex domain of the eigenvalues of the operator $\mathbf{M}$, in a set of points which is known to have some maximal properties. In this way, the interpolating polynomial is 'almost best'. The spatial derivative terms are computed by means of the Fourier method (Kosloff & Baysal 1982). The advantages of this new algorithm over finite differencing in time can be found in Tal-Ezer, Carcione & Kosloff (1989).

## 2-D WAVE PROPAGATION

For simplicity a 2-D TIV medium with symmetry axis parallel to the $z$-axis is considered. Then, the rotation matrix $\mathbf{T}$ is the identity matrix. The rheological relation is given by equation (9), with $c_{15}=c_{35}=0$. Choosing one relaxation mechanism for each mode ($L_1=L_2=1$) the unknown variable vector is given by (see Appendix D in microfiche),

$$\mathbf{U}^{\mathrm{T}}=(u_x,u_z,\dot{u}_x,\dot{u}_z,e_1,e_2,e_3), \tag{27}$$

where $e_1=e_{11}^{(1)}+e_{31}^{(1)}$, $e_2=e_{11}^{(2)}-e_{31}^{(2)}$, and $e_3=e_{51}^{(2)}$ in terms of the memory variables (20). The body forces vector is

$$\mathbf{F}^{\mathrm{T}}=(0,0,f_x/\rho,f_z/\rho,0,0,0), \tag{28}$$

and the spatial operator

$$\mathbf{M}=\begin{pmatrix} 0 & 0 & 1 & 0 & 0 & 0 & 0\\ 0 & 0 & 0 & 1 & 0 & 0 & 0\\ M_{31} & M_{32} & 0 & 0 & M_{35} & M_{36} & M_{37}\\ M_{41} & M_{42} & 0 & 0 & M_{45} & M_{46} & M_{47}\\ M_{51} & M_{52} & 0 & 0 & M_{55} & 0 & 0\\ M_{61} & M_{62} & 0 & 0 & 0 & M_{66} & 0\\ M_{71} & M_{72} & 0 & 0 & 0 & 0 & M_{77}\end{pmatrix}, \tag{29}$$

with

$$\rho M_{31}=\partial/\partial x[(c_{11}-D)+(D-c_{55})M_{u1}+c_{55}M_{u2}]\,\partial/\partial x + \partial/\partial z(c_{55}M_{u2})\,\partial/\partial z, \tag{30a}$$

$$\rho M_{32}=\partial/\partial x[(c_{13}+2c_{55}-D)+(D-c_{55})M_{u1}-c_{55}M_{u2}] \times \partial/\partial z+\partial/\partial z(c_{55}M_{u2})\,\partial/\partial x, \tag{30b}$$

$$\rho M_{35}=\partial/\partial x(D-c_{55}),\quad \rho M_{36}=\partial/\partial x c_{55},\quad \rho M_{37}=\partial/\partial z c_{55}, \tag{30c}$$

$$\rho M_{41}=\partial/\partial z[(c_{13}+2c_{55}-D)+(D-c_{55})M_{u1}-c_{55}M_{u2}] \times \partial/\partial z+\partial/\partial x(c_{55}M_{u2})\,\partial/\partial z, \tag{30d}$$

$$\rho M_{42}=\partial/\partial z[(c_{33}-D)+(D-c_{55})M_{u1}+c_{55}M_{u2}]\,\partial/\partial z + \partial/\partial x(c_{55}M_{u2})\,\partial/\partial x, \tag{30e}$$

$$\rho M_{45}=\partial/\partial z(D-c_{55}),\quad \rho M_{46}=-\partial/\partial z c_{55},\quad \rho M_{47}=\partial/\partial x c_{55}, \tag{30f}$$

$$M_{51}=\varphi_1(0)\,\partial/\partial x,\quad M_{52}=\varphi_1(0)\,\partial/\partial z,\quad M_{55}=-1/\tau_\sigma^{(1)}, \tag{30g}$$

$$M_{61}=\varphi_2(0)\,\partial/\partial x,\quad M_{62}=\varphi_2(0)\,\partial/\partial z,\quad M_{66}=-1/\tau_\sigma^{(2)}, \tag{30h}$$

and

$$M_{71}=\varphi_2(0)\,\partial/\partial z,\quad M_{72}=\varphi_2(0)\,\partial/\partial x,\quad M_{77}=-1/\tau_\sigma^{(2)}, \tag{30i}$$

where the sub-index $l$ denoting a physical mechanism has been omitted for simplicity. For a general number of physical mechanisms the number of memory variables is given by $n_v=L_1+2L_2$. The examples presented in the next section, for instance, use $L_1=L_2=2$; therefore $n_v=6$. The spatial operator for an elastic solid is obtained by taking the limit $M_{uv}\rightarrow 1$, $\varphi_v(0)\rightarrow 0$, $v=1,2$.

## EXAMPLES

The first example involves wave propagation in 2-D homogeneous TIV media, a clayshale and a sandstone whose material properties are given in Table 1. The relaxation times give almost constant $Q$ in the exploration seismic band. Similar materials with moderate to large amounts of absorption were reported by Mc Donal *et al.* (1958) for Pierre shale ($Q_\mathrm{P}=10$), and ocean bottom sediments by Hamilton *et al.* (1970), with $Q_\mathrm{P}$ ranging from 1 to 5. Isotropic versions are obtained by choosing the isotropic compressional and shear wave velocities as the pure longitudinal and pure transverse velocities (vertical direction) of the anisotropic material. The elasticities for the isotropic media are given in Table 1.

This section shows results for homogeneous clayshale and Appendix E (see microfiche) for homogeneous sandstone.

**Table 1.** Material properties of the TIV media.

| Medium | Elasticities and density | | | | | | |
|---|---|---|---|---|---|---|---|
| | $c_{11}$ ($GPa$) | $c_{12}$ ($GPa$) | $c_{13}$ ($GPa$) | $c_{33}$ ($GPa$) | $c_{55}$ ($GPa$) | $c_{66}$ ($GPa$) | $\rho$ ($Kg/m^3$) |
| *ANI Clayshale* | 66.6 | 19.7 | 39.4 | 39.9 | 10.9 | 23.4 | 2590. |
| *ANI Sandstone* | 80.2 | 25.2 | −5.0 | 80.2 | 27.9 | 27.5 | 2690. |
| *ISO Clayshale* | 39.9 | 18.1 | 18.1 | 39.9 | 10.9 | 10.9 | 2590. |
| *ISO Sandstone* | 80.2 | 24.4 | 24.4 | 80.2 | 27.9 | 27.9 | 2690. |

Relaxation times

| | $l$ | $\tau_{\epsilon l}^{(1)}$ ($s$) | $\tau_{\sigma l}^{(1)}$ ($s$) | $\tau_{\epsilon l}^{(2)}$ ($s$) | $\tau_{\sigma l}^{(2)}$ ($s$) |
|---|---|---|---|---|---|
| *Clayshale* | 1 | 0.0332577 | 0.0304655 | 0.0352443 | 0.0287482 |
| | 2 | 0.0033257 | 0.0030465 | 0.0029370 | 0.0023957 |
| *Sandstone* | 1 | 0.0325305 | 0.0311465 | 0.0332577 | 0.0304655 |
| | 2 | 0.0032530 | 0.0031146 | 0.0033257 | 0.0030465 |

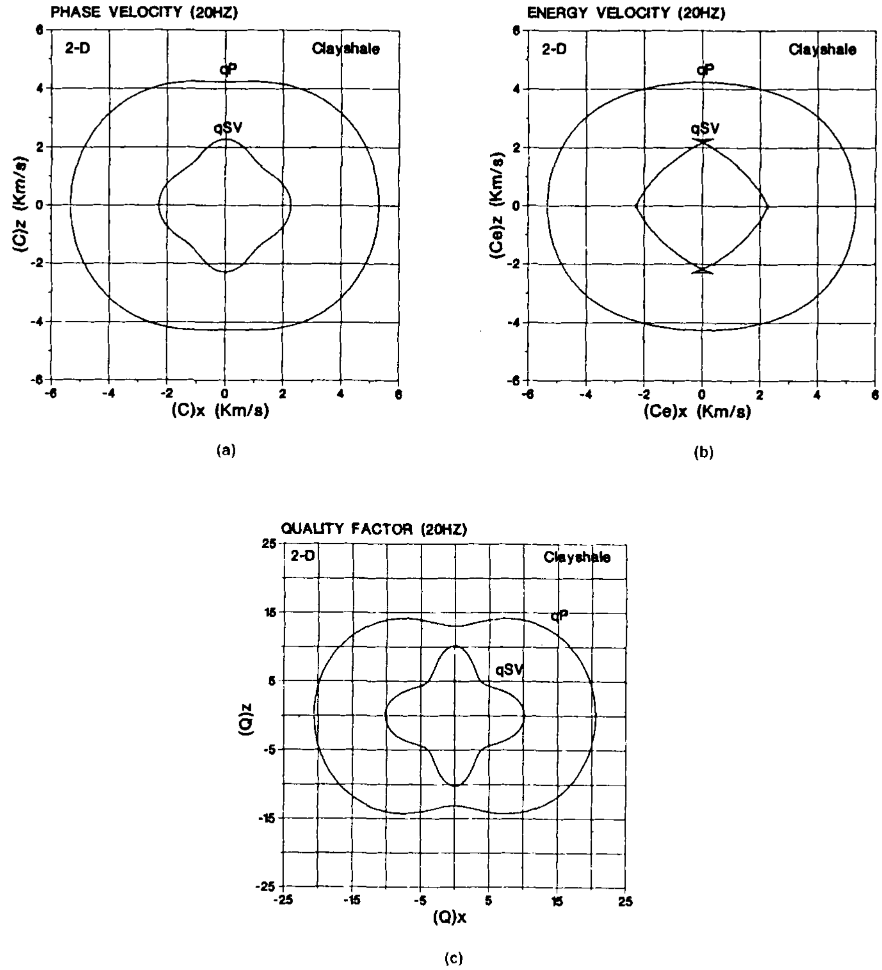


**Figure 1.** 2-D TIV clayshale, (a) phase velocity, (b) energy velocity curves (wavefronts), (c) quality factor curves. Frequency is 20 Hz. At the low- and high-frequency limits the energy velocities present minimum and maximum values respectively, while the quality factors are infinity. More details can be found in Appendix B (microfiche).

Fig. 1 displays polar representations of (a) phase velocity, (b) energy velocity, and (c) quality factors, at a frequency of $f = 20$ Hz. The expressions for these quantities are given in Appendix B with a complete analysis of the 3-D case for the same materials. The energy velocity curves present sections of the wavefront. As can be seen in Figs 1(a) and (c) the quality factor curves follow approximately the shape of the phase velocity curves.

The modelling uses a $165 \times 165$ grid mesh with $DX = DZ = 20$ m grid spacing. The motion is initiated by a vertical impulsive force located in the centre of the homogeneous region. The time function is given by

$$h(t) = e^{1/2f_0^2(t-t_0)^2} \cos\,[\pi f_0(t - t_0)], \qquad (31)$$

where $t_0 = 0.06$ s, and $f_0 = 50$ Hz is the cut-off frequency. This wavelet resembles a vibrator signal after the autocorrelation.

Figures 2 and 3 display the $u_x$ and $u_z$ components at $t = 0.32$ s for the different rheologies. The number between parenthesis denotes the plotting scale. The viscoelastic amplitudes are taken as references; scale 10 means that the amplitudes are reduced by a factor 10. All the wavefronts show the characteristics predicted by the theory. In the elastic case the shear wave amplitude is much stronger than the compressional wave amplitude, while in the anelastic case these amplitudes are comparable (except in the cusps) due to the higher attenuation acting on the shear mode. As predicted by the energy velocity curve, the anelastic wavefronts are greater than the elastic wavefronts, and the waveform appears broader due to the velocity dispersion. This dispersion effect is manifested also in the low amplitude tails following the $qP$- and $qSV$-wavefronts. The differences between the elastic and anelastic wavefronts have to be considered in relative terms. If the elastic limit is chosen in the high-frequency limit, the elastic wavefronts appear bigger than the anelastic wavefronts. A comparison between the AV and IE snapshots show important differences in amplitude, waveshape and arrival time. In some directions the anisotropic and anelastic effects compensate each other to give approximately the same arrival time in both cases (for instance at the angle $\theta = \pi/4$).

Since there is no analytical solution for the AV wave propagation problem, it is not possible, as with the other rheologies, to test the accuracy of the algorithm. As a reference, the AE $u_z$ component in the symmetry axis is compared to analytical solution (see Carcione *et al.* 1988d). As Fig. 4 shows, the comparison is excellent. From Fig. 2 the $u_x$ component along the symmetry axis is zero according

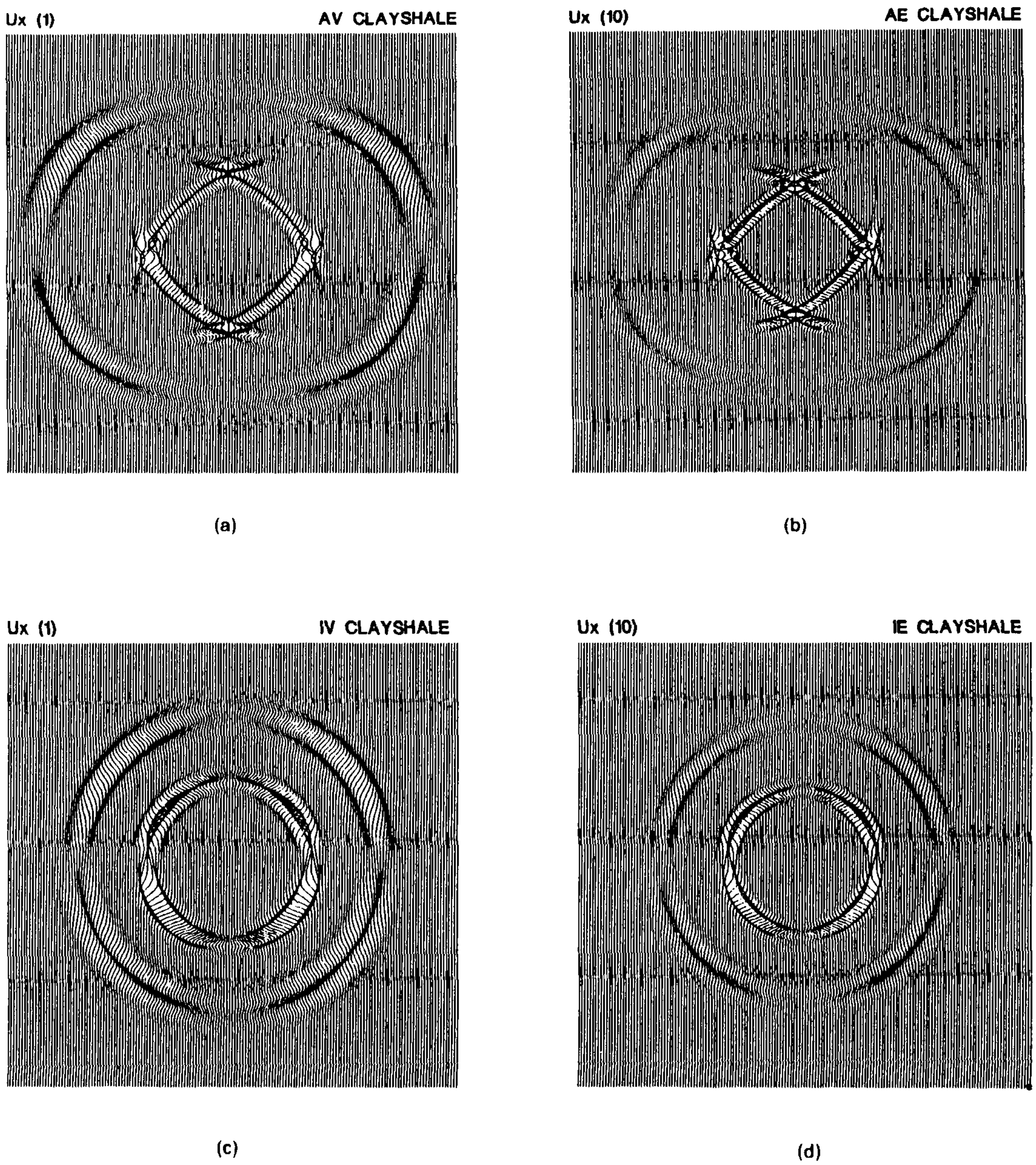


**Figure 2.** $u_x$ component of the wavefield at $t = 0.32$ s for TIV clayshale, (a) AV rheology, (b) AE rheology, (c) IV rheology, (d) IE rheology. The motion is initiated by a vertical source. The number between parenthesis denotes the plotting scale. The elastic amplitudes are reduced by a factor 10 relative to the viscoelastic amplitudes.

to the analytical solution. The same accuracy in the AV case is expected.

Synthetic seismogram comparisons in the symmetry axis at distances of 100 and 200 m from the source are displayed in Figs 5 and 6 for the $u_z$ component. At 100 m the anelastic effects produce a destructive interference between the $qP$ and $qSV$ modes, and the AV solution looks quite different compared to the other solutions. At 200 m the two modes start to separate and it is evident that the shear mode is relatively faster than the compressional mode. Although the symmetry axis is a pure mode direction, the differences in amplitude and waveform between the AV solution and the other solutions are important. Figs 7(a) and (b) display the comparison between the $u_z$ component of AE and AV clayshale in the symmetry axis and at $\theta = \pi/4$ respectively. The stations are located at 400 m from the source in both cases. As indicated by the quality factor in Fig. 1, the $qSV$ mode is more attenuated at $\theta = \pi/4$ than in the symmetry axis; while for the $qP$ mode the opposite behaviour occurs. These effects can be appreciated in Fig. 7.

A final example illustrates wave propagation in an inhomogeneous medium. An interface separates two half-spaces; the upper medium is TIV sandstone with the symmetry axis making an angle $\beta = \pi/4$ with the vertical axis, and the lower medium is IE sandstone. The source is located on the interface and has the symmetry axis direction. To solve the problem the rotation has been applied to the elasticity matrix **C**. As in the previous example the formulation requires three memory variables. Figs 8(a) and (b) display the $u_x$ and $u_z$ components at

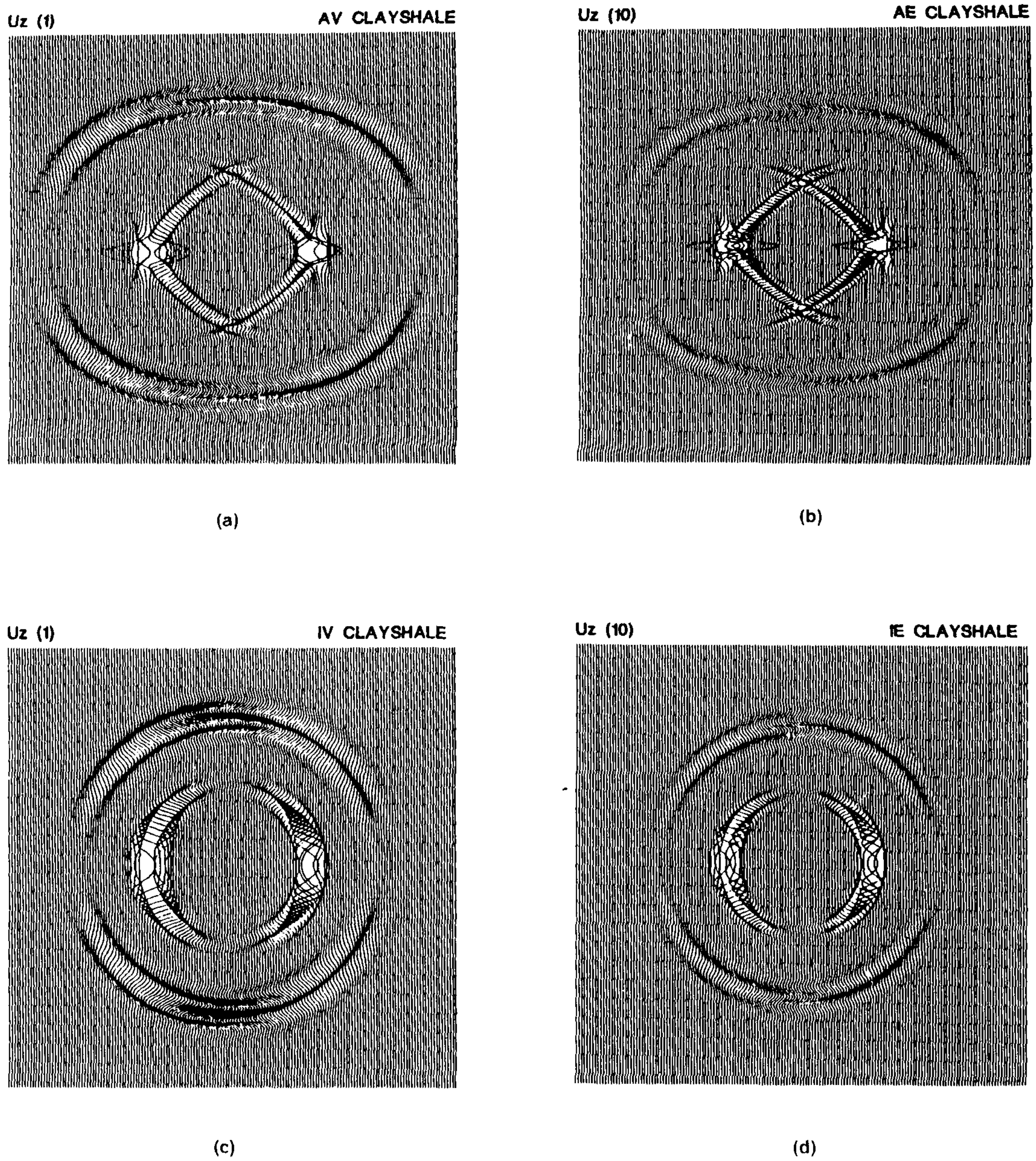


**Figure 3.** $u_z$ component of the wavefield at $t = 0.32$ s for TIV clayshale, (a) AV rheology, (b) AE rheology, (c) IV rheology, (d) IE rheology. The motion is initiated by a vertical source. The number between parenthesis denotes the plotting scale. The elastic amplitudes are reduced by a factor 10 relative to the viscoelastic amplitudes.

$t = 0.32$ s. The diagonal line indicates the symmetry axis direction. The wave characteristics in the upper medium are similar to those when $\beta = 0$ (no rotation, see Appendix E). However, as mentioned before, in order to obtain the same solution the rotation should be applied to the relaxation matrix.

## CONCLUSIONS

A general theory for describing wave propagation in anisotropic linear viscoelastic media requires the use of Boltzmann's superposition principle. Two kernels are sufficient to establish the anelastic characteristics of the wavefield; one of them is identified with the quasi-dilatational mode and the other with the quasi-shear modes. The resulting rheological relation provides the framework for computing numerical anisotropic–viscoelastic wavefields.

An analysis of a transversely isotropic–viscoelastic medium by considering homogeneous waves reveals the wave characteristics. Each frequency component has a different non-spherical wavefront. The energy and group velocities coincide only at the low- and high-frequency limits. Quality factors and velocity dispersion are not isotropic. As in the elastic anisotropic case the wavenumber vector is normal to the wavefront, and the energy velocity vector is normal the phase velocity surface.

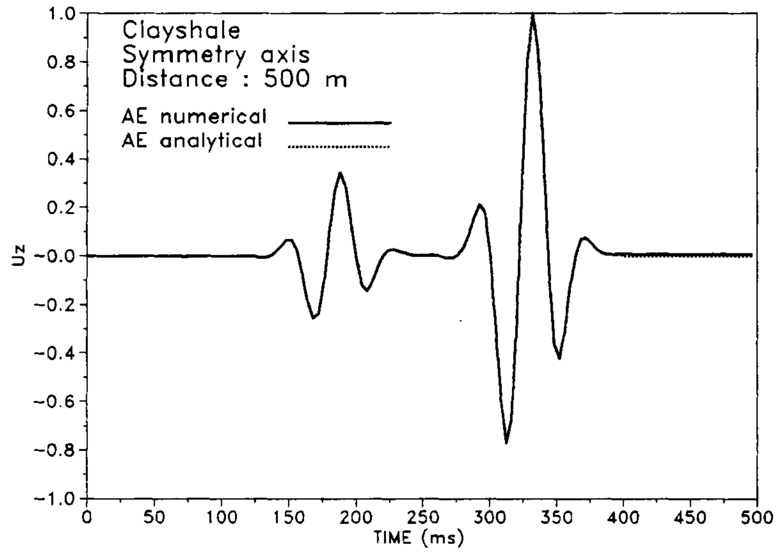


**Figure 4.** Time history comparison between the analytical and numerical AE solutions at the symmetry axis. Material is clayshale. The station is located at a distance of 500 m from the source.

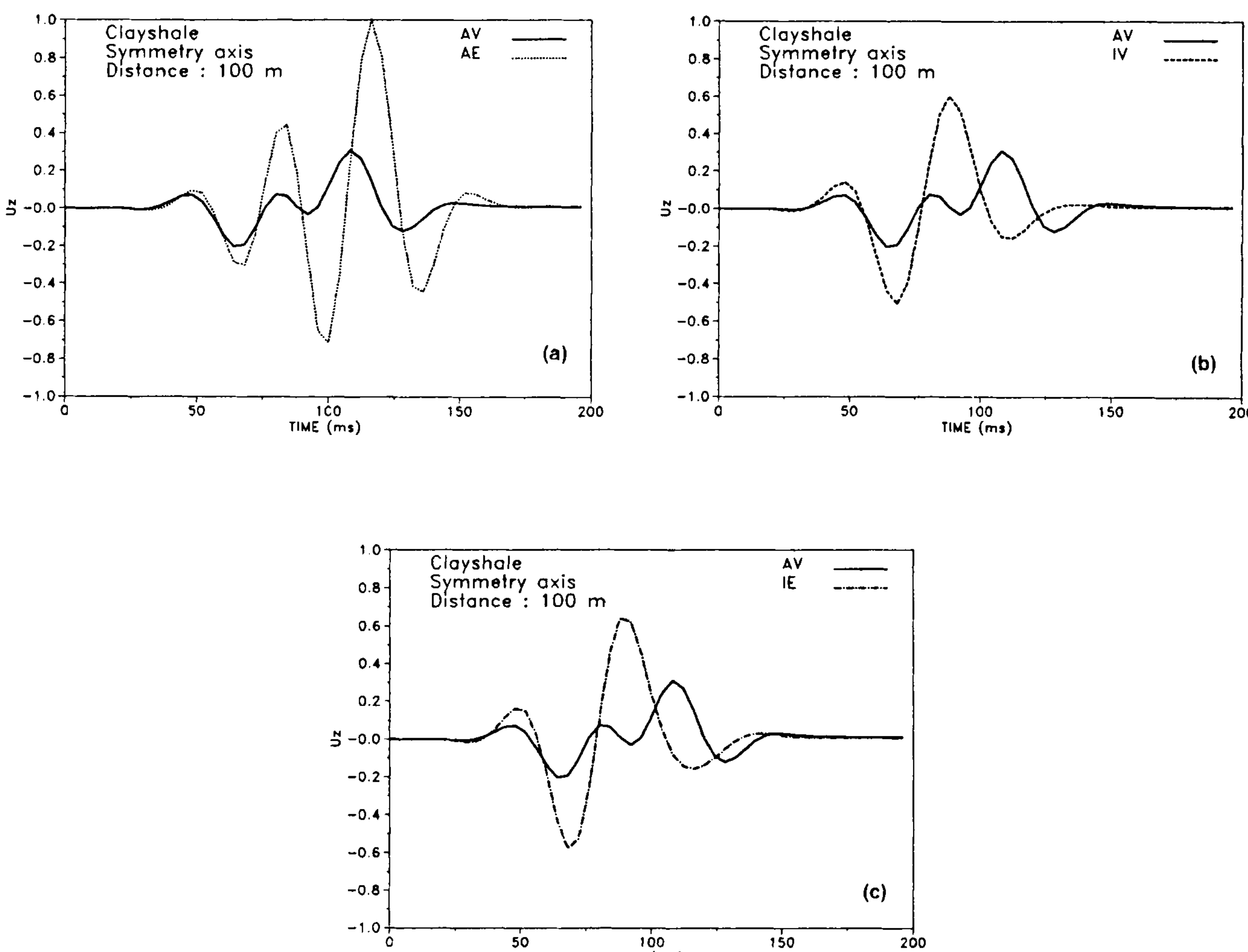


**Figure 5.** Time history comparison between the numerical AV rheology at the symmetry axis and: (a) AE rheology, (b) IV rheology, (c) IE rheology. Material is claysahle. The station is located at a distance of 100 m from the source.

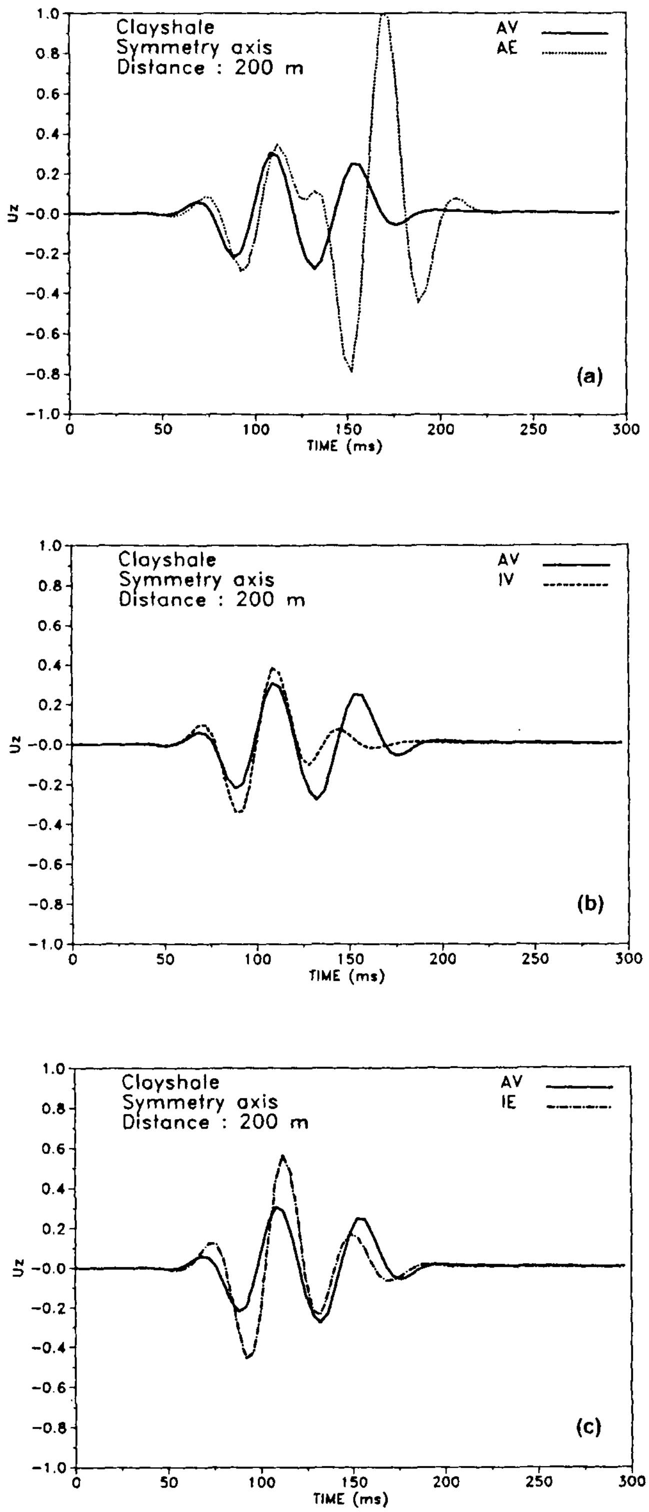


**Figure 6.** Time history comparison between the numerical AV rheology at the symmetry axis and (a) AE rheology, (b) IV rheology, (c) IE rheology. Material is clayshale. The station is located at a distance of 200 m from the source.

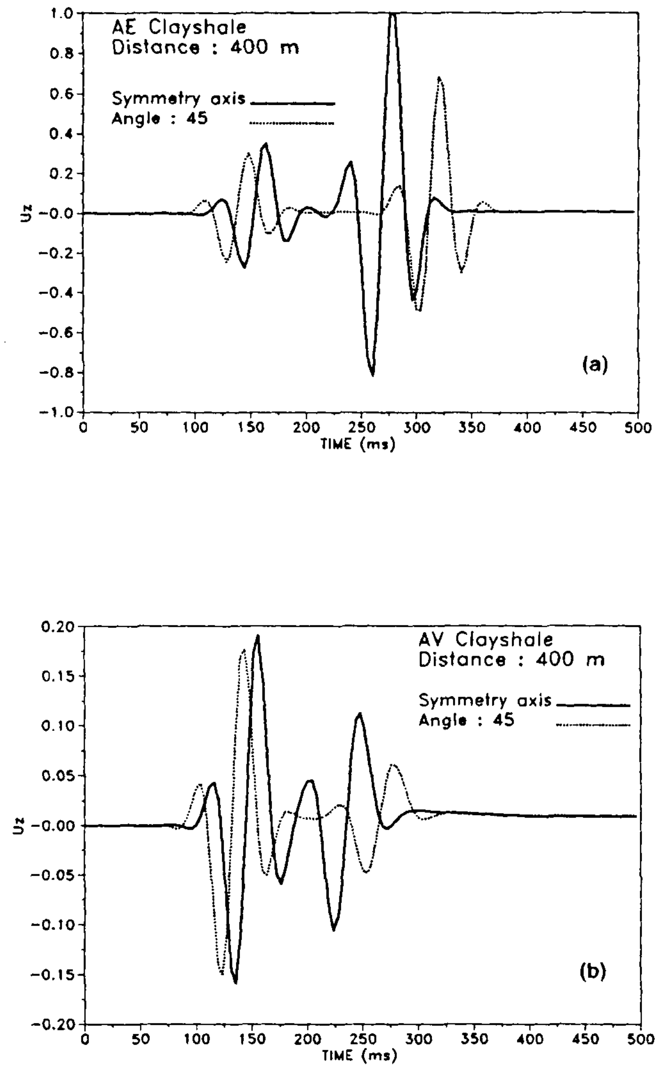


**Figure 7.** Time history comparison between two stations located at a distance of 400 m from the source, in the symmetry axis and at $\theta = \pi/4$, respectively, (a) AE rheology, (b) AV rheology. Material is clayshale.

The problem of implementing Boltzmann's superposition principle in the equation of motion is solved by assuming frequency-domain rational kernels. In this way the time-domain equation of motion can be written in differential form by introducing additional variables in the formulation. The examples show wave propagation in 2-D transversely isotropic–viscoelastic clayshale and sandstone compared with the isotropic and elastic rheologies. The simulations show the characteristics predicted by the theory, i.e., anisotropic attenuation and velocity dispersion, and important differences in waveform, amplitude and arrival time compared to the more simple rheologies.

The simulation theory presented in this paper could be the basis for developing realistic forward modelling codes; for instance, reflection and refraction surveys, vertical seismic profile, well to well propagation, etc. Another potential application is in earthquake modelling where anelastic and anisotropic effects can be expected to play a significant role if low $Q$ anisotropic layers are present.

## ACKNOWLEDGMENTS

The author wishes to thank the Alexander von Humboldt Foundation which enabled him to carry out this work at

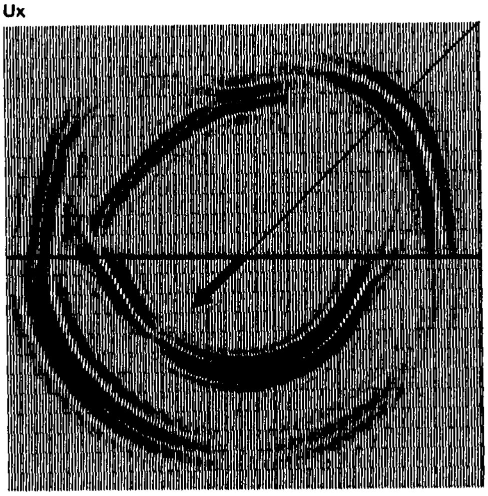


(a)

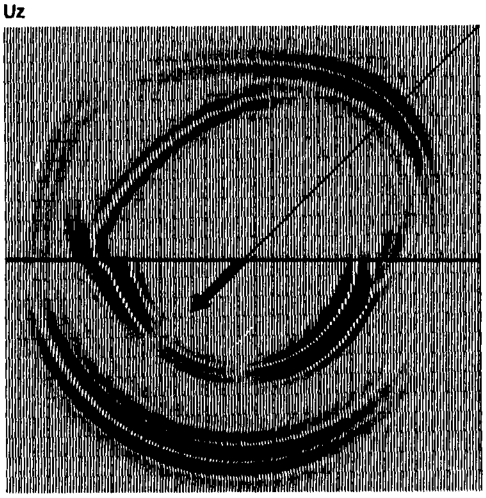


(b)

**Figure 8.** Snapshots at $t = 0.32$ s for an inhomogeneous medium composed of TIV sandstone (upper half-space) and IE sandstone (lower half-space), (a) $u_x$ component, (b) $u_z$ component. The sandstone symmetry axis and the directional force make an angle $\beta = \pi/4$ with the vertical axis. The source time history is given by equation (31).

Hamburg University. Thanks to Dr D. Kosloff and Professor A. Behle for fruitful discussions, and to the reviewers for helpful comments on the manuscript. Part of this work was supported by project EOS (Exploration Oriented Seismic Modelling and Inversion), part of Section 3.1.1.B of Joule Research and Development Programme of the Commission of the European Communities.

## REFERENCES

Alekseev, A. S. & Mikhailenko, B. G., 1980. The solution of dynamics problems of elastic wave propagation in inhomogeneous media by a combination of partial separation of variables and finite difference methods, *J. Geophys.*, **48,** 161–172.

Biot, M. A., 1962. Generalized theory of acoustic propagation in porous dissipative media, *J. Acoust. Soc. Am.*, **34,** 1254–1264.

Booth, D. C. & Crampin, S., 1983. The anisotropic reflectivity technique: theory, *Geophys. J. R. astr. Soc.*, **72,** 755–766.

Borcherdt, R. D. & Wennerberg, L., 1985, General *P*, type-*I S*, and type-*II S* waves in anelastic solids; inhomogeneous wavefields in low-loss solids, *Bull. seism. Soc. Am.*, **75,** 1729–1763.

Buchen, P. W., 1971. Plane waves in linear viscoelastic media, *Geophys. J. R. astr. Soc.*, **23,** 531–542.

Carcione, J. M., Kosloff, D. & Kosloff, R., 1988a. Wave propagation simulation in a linear viscoacoustic medium, *Geophys. J. R. astr. Soc.*, **93,** 393–407.

Carcione, J. M., Kosloff, D. & Kosloff, R., 1988b. Viscoacoustic wave propagation simulation in the earth, *Geophysics*, **53,** 769–777.

Carcione, J. M., Kosloff, D. & Kosloff, R., 1988c. Wave propagation simulation in a linear viscoelastic medium, *Geophys. J. R. astr. Soc.*, **95,** 597–611.

Carcione, J. M., Kosloff, D. & Kosloff, R., 1988d. Wave propagation simulation in an anisotropic (transversely isotropic) medium, *Q. J. Mech. Appl. Math.*, **41,** 319–345.

Christensen, R. M., 1982. *Theory of Viscoelasticity, an Introduction*, Academic Press, New York.

Crampin, S., 1985. Evaluation of anisotropy by shear-wave splitting, *Geophysics*, **50,** 142–152.

Day, S. M. & Minster, J. B., 1984. Numerical simulation of attenuated wavefields using a Pade approximant method, *Geophys. J. R. astr. Soc.*, **78,** 105–118.

Emmerich, H. & Korn, M., 1987. Incorporation of attenuation into time-domain computations of seismic wave fields, *Geophysics*, **52,** 1252–1264.

Fryer, G. J. & Frazer, N., 1987. Seismic waves in stratified anisotropic media—II. Elastodynamic eigensolutions for some anisotropic solids, *Geophys. J. R. astr. Soc.*, **91,** 73–101.

Gajewski, D. & Pšenčík, I., 1988. Ray synthetic seismograms for a 3-D anisotropic lithospheric structure, *Phys. Earth planet. Inter.*, **51,** 1–23.

Geertsma, J. & Smit, D. C., 1961. Some aspects of elastic wave propagation in fluid-saturated porous solids, *Geophysics*, **26,** 169–181.

Hamilton, E. L., Buchen, H. P., Keir, D. L. & Whitney, J. A., 1970. Velocities of compressional and shear waves in marine sediments determined in situ and from a research submarine, *J. geophys. Res.*, **75,** 4039–4049.

Jones, T. D., 1986. Pore fluids and frequency-dependent wave propagation in rocks, *Geophysics*, **51,** 1939–1953.

Kosloff, D. & Baysal, E., 1982. Forward modeling by a Fourier method, *Geophysics*, **47,** 1402–1412.

Kosloff, D., Reshef, M. & Loewenthal, D., 1984. Elastic waves calculations by the Fourier method, *Bull. seism. Soc. Am.*, **74,** 875–891.

Krebes, E. S. & Hron, F., 1980. Ray-synthetic seismograms for *SH*-waves in anelastic media, *Bull. seism. Soc. Am.*, **70,** 29–46.

Kummer, B., Behle, A. & Dorau, F., 1987. Hybrid modeling of elastic-wave propagation in two-dimensional laterally inhomogeneous media, *Geophysics*, **52,** 765–771.

Lamb, J. & Richter, J., 1966. Anisotropic acoustic attenuation with new measurements for quartz at room temperatures, *Proc. R. Soc. Lond.*, **A293,** 479–492.

Martynov, V. N. & Mikhailenko, B. G., 1984. Numerical modelling of propagation of elastic waves in anisotropic inhomogeneous media for the half-space and the sphere, *Geophys. J. R. astr. Soc.*, **76,** 53–63.

Mc Donal, F. J., Angona, F. A., Mills, R. L., Sengbush, R. L., Van Nostrand, R. G. & White, J. E., 1958. Attenuation of shear and compressional waves in Pierre shale, *Geophysics*, **23,** 421–439.

Mikhailenko, B. G., 1985. Numerical experiments in seismic investigations, *J. Geophys.*, **58,** 101–124.

Murphy, W. F., Winkler, K. W. & Kleinberg, R. L., 1986. Acoustic relaxation in sedimentary rocks: Dependence on grain contacts and fluid saturation, *Geophysics*, **51,** 757–766.

O'Connell, R. J. & Budiansky, B., 1977. Viscoelastic properties of fluid-saturated cracked solids, *J. geophys. Res.*, **82,** 5719–5735.

Szilard, J., 1982. *Ultrasonic Testing, Non-Conventional Testing Techniques,* John Wiley & Sons, New York.

Tal-Ezer, H., Carcione, J. M. & Kosloff, D., 1989. An accurate and efficient scheme for wave propagation in linear viscoelastic media, *Geophysics*, submitted.

Virieux, J., 1986. *P–SV* wave propagation in heterogeneous media: velocity–stress finite-difference method, *Geophysics,* **51,** 889-901.

White, J. E., 1982. Computed waveforms in transversely isotropic media, *Geophysics*, **47,** 771–883.

# APPENDIX A

## ANISOTROPIC LINEAR VISCOELASTIC CONSTITUTIVE RELATION

The most general relation between the components of the stress tensor $\sigma_{ij}$ and the components of the strain tensor $\varepsilon_{ij}$ for an anisotropic linear viscoelastic medium is given by (Christensen, 1982, p. 5),

$$\sigma_{ij}(\mathbf{x}, t) = \psi_{ijkl}(\mathbf{x}, t) * \dot{\varepsilon}_{kl}(\mathbf{x}, t), \quad i,j,k,l = 1,...,3 \tag{A1}$$

where $t$ is the time variable, $\mathbf{x}$ is the position vector, $\psi_{ijkl}$ are the components of a fourth order tensorial relaxation function, and the symbol '*' indicates time convolution. A dot above a variable denotes time differentiation, and the Einstein convention for repeated indices is used.

The fourth rank tensor $\Psi$ contains all the information about the behavior of the medium under infinitesimal deformations. In the most general case the number of components are 81, but since the stress and strain tensors are symmetrical, and from the positive real nature of the strain and loss in energy densities (Auld, 1973, p. 144 and 155 respectively), it follows that the number of independent components reduces to 21. Equation (A1) is the formulation of the isothermal AV stress-strain constitutive relation. This expression, also called Boltzmann's superposition principle, will be the basis for describing wave propagation in AV media.

Using the shortened matrix notation, equation (A1) can be written as equation (4). It is established now the time dependence of the relaxation components based on the general standard linear solid, assuming that

$$\psi_{IJ} = [A_{IJ} + A_{IJ}^{(1)}\chi_1 + A_{IJ}^{(2)}\chi_2]H(t) = [A_{IJ} + A_{IJ}^{(\nu)}\chi_\nu]H(t) \tag{A2}$$

where $A_{IJ}$ and $A_{IJ}^{(\nu)}$ are space-dependents functions, and $\chi_\nu(\mathbf{x}, t)$ are relaxation functions defined in equation (8), which under certain conditions that will be imposed later, correspond to states of quasi-dilatation ($\nu = 1$) , and quasi-shear ($\nu = 2$ ) respectively. It can be proved that these relaxation functions represent $L_\nu$ standard linear elements of unit relaxed modulus and a spring of constant $(1 - L_\nu)$ all connected in parallel (see for instance Ben-Menahem and Singh, 1981, p. 856, for the equation of a single element and the physical meaning of the relaxation times). This type of relaxation function was introduced by Liu et al., (1976). Despite the negative value of the spring constant the model has positive relaxed and unrelaxed moduli. In terms of mechanical models the relaxation components defined in (A2) represent a spring ($A_{IJ}H(t)$), plus $L_1$ standard linear elements for quasi-dilatation states, and $L_2$ standard linear elements for quasi-shear deformation.

Replacing (A2) in (4) gives equation (5). In order to identify $\chi_1$ with the quasi-dilatational field and $\chi_2$ with the quasi-shear field, the following conditions are imposed:

**Condition 1:** The mean stress depends on the time variable only through the function $\chi_1$,

$$\Theta_\sigma \equiv \frac{1}{3}\sum_{I=1}^{3} T_I[\chi_1(t)], \tag{A3}$$

**Condition 2:** In a given system of coordinates $S$ the deviatoric components of the stress tensor depend on the time variable only through the function $\chi_2$,

$$T_I - \Theta_\sigma = (T_I - \Theta_\sigma)[\chi_2(t)], \quad I \leq 3, \tag{A4a}$$

$$T_I = T_I[\chi_2(t)], \quad I > 3, \tag{A4b}$$

The trace of the stress tensor is invariant under transformations of the system of coordinates. This fact ensures that the mean tension is related only to the function $\chi_1$ in any system. The deviatoric components are not invariant, but Condition 2 implies that a cube of material orientated in the direction of the axes of the system $S$ will be subjected to shear deformations exclusively related to the function $\chi_2$ With condition 2 the value of the shear quality factors in the symmetry axis direction of a TIV medium as shown in Appendix B can be established.

Substituting (5) in (A3) the mean stress is

$$\Theta_\sigma = \frac{1}{3}\left[\left(\sum_{I=1}^{3} A_{IJ} + \chi_1\sum_{I=1}^{3} A_{IJ}^{(1)} + \chi_2\sum_{I=1}^{3} A_{IJ}^{(2)}\right)H(t)\right]*\dot{S}_J, \tag{A5}$$

Hence, Condition 1 implies

$$\sum_{I=1}^{3} A_{IJ}^{(2)} = 0 \quad J = 1,...,6 \tag{A6}$$

Condition 2 implies

$$A_{IJ}^{(1)} = \frac{1}{3}\left[\sum_{K=1}^{3} A_{KJ}^{(1)}\right], \quad I \leq 3, \quad J = 1,...,6 \tag{A7a}$$

and

$$A_{IJ}^{(1)} = 0, \quad I > 3, \quad J = 1,\ldots,6 \tag{A7b}$$

which follow from (A4a) and (A4b) respectively. Two additional conditions are imposed to the relaxation components:

**Condition 3:** In the AE limit the relaxation matrix must give the elasticity matrix,

$$\underset{\sim}{\Psi} \rightarrow \underset{\sim}{C} = \begin{bmatrix} c_{11} & c_{12} & c_{13} & c_{14} & c_{15} & c_{16} \\ & c_{22} & c_{23} & c_{24} & c_{25} & c_{26} \\ & & c_{33} & c_{34} & c_{35} & c_{36} \\ & & & c_{44} & c_{45} & c_{46} \\ & & & & c_{55} & c_{56} \\ & & & & & c_{66} \end{bmatrix} H, \tag{A8}$$

In this way the elasticities are identified with the relaxed components of the relaxation matrix, which are obtained in the limit $t \rightarrow \infty$ in equation (8), i.e., $\chi_\nu \rightarrow 1$ in (A2). Note that the elastic limit is also equivalent to $\tau_{\varepsilon l}^{(\nu)} \rightarrow \tau_{\sigma l}^{(\nu)}$, and particularly when $\tau_{\varepsilon l}^{(\nu)} \rightarrow \tau_{\sigma l}^{(\nu)} \rightarrow 0$, which is consistent with the elimination of the dashpots if one thinks in terms of mechanical models. Also, for some microstructural theories (see Murphy et al., 1986; O'Connel and Budiansky, 1977) the complex moduli depend on the frequency $\omega$ and the fluid viscosity $\eta$ as $\omega\eta$ Therefore, elastic material means here to consider a zero viscosity fluid, which is equivalent to taking the low-frequency limit. For Biot's theory for instance, zero viscosity is equivalent to the high-frequency limit, since the complex moduli depend of $\omega\eta^{-1}$ (see Geertsma and Smit, 1961).

**Condition 4:** In the IV limit the relaxation matrix must give the isotropic-viscoelastic matrix (Carcione et al., 1988c),

$$\underset{\sim}{\Psi} \rightarrow \underset{\sim}{\Psi}^I = \begin{bmatrix} \psi_{11}^I & \psi_{12}^I & \psi_{12}^I & 0 & 0 & 0 \\ & \psi_{11}^I & \psi_{12}^I & 0 & 0 & 0 \\ & & \psi_{11}^I & 0 & 0 & 0 \\ & & & \psi_{44}^I & 0 & 0 \\ & & & & \psi_{44}^I & 0 \\ & & & & & \psi_{44}^I \end{bmatrix} H, \tag{A9}$$

where

$$\psi_{11}^I = \left(\lambda^e + \frac{2}{n}\mu^e\right)\chi_1 + \frac{2}{n}(n-1)\mu^e\chi_2, \tag{A10a}$$

$$\psi_{12}^I = \left(\lambda^e + \frac{2}{n}\mu^e\right)\chi_1 - \frac{2}{n}\mu^e\chi_2, \tag{A10b}$$

and

$$\psi_{44}^I = \mu^e\chi_2, \tag{A10c}$$

with $\lambda^e$ and $\mu^e$ the elastic Lame constants and $n$ the dimension of the space.

An example of a 3-D relaxation matrix subject to Conditions 1 to 4 is obtained by taking

$$A_{11} = c_{11} - D, \quad A_{22} = c_{22} - D, \quad A_{33} = c_{33} - D,$$

$$A_{44} = A_{55} = A_{66} = A_{44}^{(1)} = A_{5}^{(1)} = A_{66}^{(1)} = 0,$$

$$A_{11}^{(1)} = A_{22}^{(1)} = A_{33}^{(1)} = D - \frac{4}{3}G,$$

$$A_{11}^{(2)} = A_{22}^{(2)} = A_{33}^{(2)} = \frac{4}{3}G,$$

and

$$A_{22}^{(2)} = c_{44}, \quad A_{55}^{(2)} = c_{55}, \quad A_{66}^{(2)} = c_{66},$$

for the diagonal elements, and

$$A_{12} = c_{12} - D + 2G, \quad A_{13} = c_{13} - D + 2G, \quad A_{23} = c_{23} - D + 2G,$$

$$A_{12}^{(1)} = A_{13}^{(1)} = A_{23}^{(1)} = D - \frac{4}{3}G,$$

$$A_{12}^{(2)} = A_{13}^{(2)} = A_{23}^{(2)} = -\frac{2}{3}G,$$

$$A_{14}^{(1)} = A_{14}^{(2)} = A_{15}^{(1)} = A_{15}^{(2)} = A_{16}^{(1)} = A_{16}^{(2)} = 0,$$

$$A_{14} = c_{14}, \quad A_{15} = c_{15}, \quad A_{16} = c_{16},$$

$$A_{24}^{(1)} = A_{24}^{(2)} = A_{25}^{(1)} = A_{25}^{(2)} = A_{26}^{(1)} = A_{26}^{(2)} = 0,$$

$$A_{24} = c_{24}, \quad A_{25} = c_{25}, \quad A_{26} = c_{26},$$

$$A_{34}^{(1)} = A_{34}^{(2)} = A_{35}^{(1)} = A_{35}^{(2)} = A_{36}^{(1)} = A_{36}^{(2)} = 0,$$

$$A_{34} = c_{34}, \quad A_{35} = c_{35}, \quad A_{36} = c_{36},$$

$$A_{45} = A_{46} = A_{56} = A_{45}^{(1)} = A_{46}^{(1)} = A_{56}^{(1)} = 0,$$

and

$$A_{45}^{(2)} = c_{45}, \quad A_{46}^{(2)} = c_{46}, \quad A_{56}^{(2)} = c_{56},$$

for the off-diagonal elements. Substitution of this expressions into (A2) gives the relaxation matrix (6). In a similar way the relaxation matrix (9) for the 2-D case is obtained.
For the 3-D case the mean stress (A3) becomes

$$\Theta_\sigma = \frac{1}{3}(c_{J1} + c_{J2} + c_{J3})S_J + 3\left(D - \frac{4}{3}G\right)\dot{\Theta}_\varepsilon * [(\chi_1 - 1)H], \tag{A11}$$

where

$$\Theta_\varepsilon \equiv \frac{\varepsilon_{II}}{3} = \frac{1}{3}\sum_{I=1}^{3} S_I, \tag{A12}$$

is the mean strain. As can be seen, equation (A11) satisfies Condition 1. The deviatoric components of the stress tensor are

$$T_I - \Theta_\sigma = \sum_{K=1}^{3}\left(\delta_{IK} - \frac{1}{3}\right)c_{KJ}S_J + 2G(\dot{S}_I - \dot{\Theta}_\varepsilon) * [(\chi_2 - 1)H], \quad I \leq 3, \tag{A13a}$$

with $\delta_{IK}$ the Kronecker delta, and

$$T_I = \sum_{J=1}^{3} c_{IJ}S_J + \sum_{J=4}^{6} c_{IJ}[(\chi_2 H) * \dot{S}_J], \quad I > 3, \tag{A13b}$$

which satisfy Condition 2.
In the AE limit, $\tau_{\varepsilon l}^{(\nu)} \to \tau_{\sigma l}^{(\nu)}$, $l = 1, \ldots, L_\nu$, therefore from equation (8) $\chi_\nu \to 1$, the mean stress (A11) reduces to

$$\Theta_\sigma = \frac{1}{3}(c_{J1} + c_{J2} + c_{J3})S_J, \tag{A14}$$

and the deviatoric components,

$$T_I - \Theta_\sigma = \sum_{K=1}^{3}\left(\delta_{IK} - \frac{1}{3}\right)c_{KJ}S_J, \quad I \leq 3 \tag{A15a}$$

and

$$T_I = c_{IJ}S_J, \quad I > 3, \tag{A15b}$$

i.e., the generalized Hooke's law.
In the IV limit the elasticities give

$$c_{11}, \ c_{22}, \ c_{33} \to \lambda^e + 2\mu^e,$$

$$c_{44}, \ c_{55}, \ c_{66} \to \mu^e,$$

$$c_{12}, \ c_{13}, \ c_{23} \to \lambda^e,$$

and zero the other components. The mean stress (A11) and deviatoric components (A13a) and (A13b) simplify to

$$\Theta_\sigma = 3\left(\lambda^e + \frac{2}{3}\mu^e\right)[\dot{\Theta}_\varepsilon * (\chi_1 H)], \tag{A15}$$

and

$$T_I - \Theta_\sigma = 2\mu^e(\dot{S}_I - \dot{\Theta}_\varepsilon) * (\chi_2 H), \quad I \leq 3, \tag{A15a}$$

$$T_I = \mu^e(\chi_2 H) * \dot{S}_I, \quad I > 3, \tag{A15b}$$

i.e., the IV rheological relation defined in Carcione et al., (1988c).
It is important to note that the relaxation matrices (6) and (9) are not unique, other choices could also satisfy the four conditions. As mentioned before, the strain and loss energy densities must be positive definite quadratic functions. These conditions impose some constraints on the rhelogical relation, which will be verified for the frequency-domain stiffness components in Appendix B.

## REFERENCES


Auld, B.A., 1973. Acoustic fields and waves in solids, Vol. 1, John Wiley & Sons, Inc., New York.

Ben-Menahem, A.B., & Singh, S.J., 1981. Seismic waves and sources, Springer Verlag, New York.

Biot, M.A., 1962. Generalized theory of acoustic propagation in porous dissipative media, J. Acoust. Soc. Am., **34**, 1254-1264.

Carcione, J.M., Kosloff, D., & Kosloff, R., 1988c. Wave propagation in a linear viscoelastic medium, Geophys. J. Roy. Astr. Soc., **95** , 597-611.

Christensen, R.M., 1982. Theory of viscoelasticity: an introduction, Academic Press Inc., New York & London, 2nd ed.

Geertsma, J., & Smit, D.C., 1961. Some aspects of elastic wave propagation in fluid-saturated porous solids, Geophysics, **26**, 169-181.

Liu, H.P., Anderson, D.L., & Kanamori, H., 1976. Velocity dispersion due to anelasticity; implications for seismology and mantle composition, Geophys. J. Roy. Astr. Soc., **47**, 41-58

Murphy, W.F., Winkler, K.W., & Kleinberg, R.L., 1986. Acoustic relaxation in sedimentary rocks: Dependence on grain contacts and fluid saturation, Geophysics, **51**, 757-766.

O'Connell, R.J. & Budiansky, B., 1977. Viscoelastic properties of fluid-saturated cracked solids, J. Geophys. Res., **82**, 5719-5735.

# APPENDIX B

## PLANE WAVE ANALYSIS OF THE AV MEDIUM

Uniform plane waves provide a very useful tool for analizing the characteristics of wave propagation. Since the analysis is in the frequency-domain, the complex stiffness matrix from the relaxation matrix is first obtained. Then, the energy conservation equation for the AV medium; afterwards, the physical velocities, phase, group and energy velocities in terms of the complex velocities, and finally the quality factors for the three different propagating modes. As a consequence, the relations among the different physical velocities and quality factors are summarized for the various rheologies.

### Frequency-domain constitutive relation

The stress-strain relation (4) can also be written as

$$T_I = \dot{\psi}_{IJ} * S_J, \quad I,J = 1,\dots,6 \tag{B1}$$

Applying the convolutional theorem to equation (B1) the rheological relation takes the form

$$\tilde{T}_I = \tilde{\dot{\psi}}_{IJ} \tilde{S}_J \equiv p_{IJ} \tilde{S}_J, \tag{B2}$$

where the tilde means time Fourier transform. Equation (B2) defines the frequency-domain stiffness matrix as

$$p_{IJ}(\omega) = \tilde{\dot{\psi}}_{IJ} \equiv r_{IJ}(\omega) + i q_{IJ}(\omega), \tag{B3}$$

with $\omega$ the angular frequency. In matrix notation equation (B3) is

$$\underset{\sim}{\mathbf{P}} = \underset{\sim}{\mathbf{R}} + i\underset{\sim}{\mathbf{Q}}, \tag{B4}$$

where

$$\underset{\sim}{\mathbf{R}} = Re[\underset{\sim}{\mathbf{P}}] \tag{B5a}$$

and

$$\underset{\sim}{\mathbf{Q}} = Im[\underset{\sim}{\mathbf{P}}] \tag{B5b}$$

are real matrices. The operators $Re$ and $Im$ take real and imaginary parts respectively.
Replacing (A2) in (B3) yields

$$p_{IJ} = A_{IJ} + A_{IJ}^{(\nu)} M_\nu, \tag{B6}$$

where

$$M_\nu = \tilde{\dot{\chi}}_\nu H \quad \nu = 1,2 \tag{B7}$$

are the adimensional complex moduli given by (Carcione et al., 1988c),

$$M_\nu = 1 - L_\nu + \sum_{l=1}^{L_\nu} \frac{1 + i\omega\tau_{\varepsilon l}^{(\nu)}}{1 + i\omega\tau_{\sigma l}^{(\nu)}}, \quad \nu = 1,2. \tag{B8}$$

From equation (B6) the real and imaginary parts of the stiffness components become

$$r_{IJ} = A_{IJ} + A_{IJ}^{(\nu)} Re[M_\nu], \tag{B9a}$$

and

$$q_{IJ} = A_{IJ}^{(\nu)} Im[M_\nu], \tag{B9b}$$

respectively. In virtue of equation (B3) the complex stiffness matrices corresponding to the constitutive relations (6) and (9) are

$$\underset{\sim}{\mathbf{P}} = \begin{bmatrix} p_{11} & p_{12} & p_{13} & c_{14} & c_{15} & c_{16} \\ & p_{22} & p_{23} & c_{24} & c_{25} & c_{26} \\ & & p_{33} & c_{34} & c_{35} & c_{36} \\ & & & c_{44}M_2 & c_{45}M_2 & c_{46}M_2 \\ & & & & c_{55}M_2 & c_{56}M_2 \\ & & & & & c_{66}M_2 \end{bmatrix}, \tag{B10}$$

where

$$p_{11} = c_{11} - D + (D - \frac{4}{3}G)M_1 + \frac{4}{3}GM_2, \tag{B11a}$$

$$p_{12} = c_{12} - D + 2G + (D - \frac{4}{3}G)M_1 - \frac{2}{3}GM_2, \tag{B11b}$$

$$p_{13} = c_{13} - D + 2G + (D - \frac{4}{3}G)M_1 - \frac{2}{3}GM_2, \tag{B11c}$$

$$p_{22} = c_{22} - D + (D - \frac{4}{3}G)M_1 + \frac{4}{3}GM_2, \tag{B11d}$$

$$p_{23} = c_{23} - D + 2G + (D - \frac{4}{3}G)M_1 - \frac{2}{3}GM_2, \tag{B11e}$$

and

$$p_{33} = c_{33} - D + (D - \frac{4}{3}G)M_1 + \frac{4}{3}GM_2, \tag{B11f}$$

in the 3-D case, and

$$\underset{\sim}{\mathbf{P}} = \begin{bmatrix} p_{11} & p_{12} & c_{15} \\ & p_{22} & c_{35} \\ & & c_{55}M_2 \end{bmatrix} H, \tag{B12}$$

where

$$p_{11} = c_{11} - D + (D - c_{55})M_1 + c_{55}M_2, \tag{B13a}$$

$$p_{12} = c_{13} + 2c_{55} - D + (D - c_{55})M_1 - c_{55}M_2, \tag{B13b}$$

and

$$p_{22} = c_{33} - D + (D - c_{55})M_1 + c_{55}M_2, \tag{B13c}$$

in the 2-D case.

## Complex Poynting's theorem

The complex Poynting's theorem for a general AV medium is given by (Auld, 1973, p. 154),

$$\int_S \mathbf{p} \cdot \hat{e}_n dS - i\omega[(E_s)_{peak} - (E_v)_{peak}] + (P_d)_{AV} = P_s, \tag{B14}$$

with $\mathbf{p}$ the complex Poynting vector defined as

$$\mathbf{p} = -\frac{1}{2}(\hat{e}_x \dot{u}_i^* \sigma_{ix} + \hat{e}_y \dot{u}_i^* \sigma_{iy} + \hat{e}_z \dot{u}_i^* \sigma_{iz}), \tag{B15}$$

where $\mathbf{u}(\mathbf{x}, t)$ is the displacement vector, and the superscript '*' denotes complex conjugate. The surface integral in (B14) is the total power flow outward in the direction of $\hat{e}_n$, through a closed surface $S$ which includes a volume $V$. The quantities

$$(E_s)_{peak} = \int_V \frac{\mathbf{S}:\underset{\sim}{\mathbf{R}}:\mathbf{S}^*}{2} dV, \tag{B16}$$

and

$$(E_v)_{peak} = \int_V \frac{\rho}{2} |\dot{\mathbf{u}}|^2 dV, \tag{B17}$$

are the peak strain energy and peak kinetic energy respectively, where $\mathbf{R}$ is given by (B5a), and $\rho$ is the density. The double dot product ':' is defined by the summation over a single abbreviated subscript. For instance,

$$\mathbf{S}:\underset{\sim}{\mathbf{R}}:\mathbf{S}^* \equiv S_I r_{IJ} S_J^*,$$

The quantity $(P_d)_{AV}$ is the time-average power loss due to anelasticity,

$$(P_d)_{AV} = \omega \int_V \frac{\mathbf{S}:\underset{\sim}{\mathbf{Q}}:\mathbf{S}^*}{2} dV, \tag{B18}$$

with $\mathbf{Q}$ given by equation (B5b). Finally, $P_s$ is the complex power supplied by the sources. Actually, Auld (1973, p. 86) considers a Kelvin-Voigt mechanical model for the constitutive relation but the procedure to obtain equation (B14) is independent of the rheological model.
From equations (B16) and (B17) the peak strain and kinetic energy densities are

$$(\varepsilon_s)_{peak} = \frac{\mathbf{S}:\underset{\sim}{\mathbf{R}}:\mathbf{S}^*}{2}, \tag{B19}$$

and

$$(\varepsilon_v)_{peak} = \frac{\rho}{2}|\dot{\mathbf{u}}|^2, \tag{B20}$$

respectively. In consequence, the average stored energy density is

$$\varepsilon_{AV} = \frac{(\varepsilon_v)_{peak} + (\varepsilon_s)_{peak}}{2} = \frac{1}{4}[\rho|\dot{\mathbf{u}}|^2 + \mathbf{S}:\underset{\sim}{\mathbf{R}}:\mathbf{S}^*]. \tag{B21}$$

From equation (B18) the loss in energy density is

$$(\varepsilon_d)_{AV} = \frac{\mathbf{S}:\underset{\sim}{\mathbf{Q}}:\mathbf{S}^*}{2}, \tag{B22}$$

The quantities which define the energy balance equation (B14) will be used in the following sections to compute the energy velocities and quality factors.
The positive definiteness of the strain and loss energy densities implies some physical realizability conditions for the real matrices $\mathbf{R}$ and $\mathbf{Q}$. By hypothesis these conditions are satisfied by the elasticity matrix $\mathbf{C}$, and since for realistic earth materials ($Q >> 1$), $\mathbf{R}$ does not differ greatly from $\mathbf{C}$ (by equation (A8) $\mathbf{C}$ is the AE limit of $\mathbf{R}$), it is reasonable to assume that $\mathbf{R}$ also satisfy the conditions. However, it is not obvious that $\mathbf{Q}$ is a positive definite matrix. The following demonstrates that the physical realizability conditions are verified for $\mathbf{Q}$ in the case of a TIV medium:

**Physical realizability conditions:** Since the strain and loss energy densities (equations (B19) and (B22) respectively) are defined as positive definite quadratic functions, the stiffness components given by equation (B6) must satisfy the following constraints (Korn and Korn, 1961),

$$d_{II} > 0, \quad \begin{bmatrix} d_{II} & d_{IJ} \\ d_{IJ} & d_{JJ} \end{bmatrix} > 0, \quad \ldots \quad \det[d_{IJ}] > 0, \tag{B23}$$

where $d_{IJ}$ represents $r_{IJ}$ or $q_{IJ}$. The example considers physical realizability conditions for the matrix $\mathbf{Q}$ in the case of a TIV medium. A sufficient set of conditions is given by (Auld, 1973, p. 147),

$$q_{11} > |q_{12}|, \tag{B24a}$$

$$q_{55} > 0, \tag{B24b}$$

and

$$(q_{11} + q_{12})q_{33} > 2q_{13}^2, \tag{B24c}$$

The adimensional complex moduli (B8) can be separated into real and imaginary parts where

$$Re[M_\nu] = 1 - L_\nu + \sum_{l=1}^{L_\nu} \frac{1 + \omega^2 \tau_{\varepsilon l}^{(\nu)} \tau_{\sigma l}^{(\nu)}}{1 + \omega^2 \tau_{\sigma l}^{(\nu)2}}, \tag{B25a}$$

and

$$Im[M_\nu] = \omega \sum_{l=1}^{L_\nu} \frac{(\tau_{\varepsilon l}^{(\nu)} - \tau_{\sigma l}^{(\nu)})}{1 + \omega^2 \tau_{\sigma l}^{(\nu)2}}, \tag{B25b}$$

for $\nu = 1,2$. Since $\tau_{\varepsilon l}^{(\nu)} > \tau_{\sigma l}^{(\nu)}$, the imaginary part of the complex moduli satisfies

$$Im[M_\nu] > 0. \tag{B26}$$

Equation (B24a) implies

$$q_{11} - q_{12} > 0, \tag{B27a}$$

and

$$q_{11} + q_{12} > 0. \tag{B27b}$$

Substracting the imaginary parts of (B11b) and (B11a) gives

$$q_{11} - q_{12} = 2G\, Im[M_2], \tag{B28}$$

which by (B26) and since $G > 0$ (see equation (7h)), satisfies equation (B27a). Adding the imaginary parts of (B11a) and (B11b) gives

$$q_{11} + q_{12} = 2\left(D - \frac{4}{3}G\right) Im[M_1] + \frac{2}{3}G\, Im[M_2]. \tag{B29}$$

For real materials, in general is $D - 4G/3 > 0$, (see for instance Table 1 with equations (7g) and (7h)). This fact and (B26) prove that equation (B29) satisfies (B27b).
The second condition (B24b) implies

$$q_{55} = c_{55}\, Im[M_2] > 0, \tag{B30}$$

which is valid by (B26) and since $c_{55} > 0$.
Finally, after substitution of the imaginary parts of equations (B11a), (B11b), (B11c) and (B11f) in condition (B24c) gives

$$6G\left(D - \frac{4}{3}G\right) Im[M_1]\, Im[M_2] > 0, \tag{B31}$$

which is valid in virtue of previous arguments. In consequence, $\mathbf{Q}$ for a TIV medium is a positive definite matrix and satisfies the physical conditions

## Christoffel equation and dispersion relation

Considering zero body forces and Fourier transforming equation (12) with respect to the time gives

$$\overline{\nabla}_{iJ}\tilde{T}_J = -\rho\omega^2\tilde{u}_i, \tag{B32}$$

Substituting $\tilde{T}_J$ from equation (B2) yields

$$\overline{\nabla}_{iJ}p_{JK}\tilde{S}_K = -\rho\omega^2\tilde{u}_i, \tag{B32}$$

or

$$\overline{\nabla}_{iJ}p_{JK}\overline{\nabla}_{Kj}\tilde{u}_j = -\rho\omega^2\tilde{u}_i, \tag{B33}$$

where $\overline{\nabla}_{Kj}$ is the transpose of the matrix defined by equation (13).
Let a plane wave solution to equation (B33) be of the form

$$\tilde{u}_l = U_l e^{-i\mathbf{k}\cdot\mathbf{x}}, \tag{B34}$$

where $\mathbf{k}$ is the complex wavenumber vector defined by

$$\mathbf{k} = \vec{\kappa} - i\vec{\alpha}, \tag{B35}$$

with $\vec{\kappa}$ and $\vec{\alpha}$ real vectors indicating the directions and magnitudes of propagation and attenuation respectively. In general, these directions are different and the wave (B34) is termed inhomogeneous, with $\vec{\kappa}\cdot\vec{\alpha}$ strictly different from zero, unlike the interface waves in elastic media. When the directions coincide the wave is called homogeneous. Alternatively, the complex wavenumber can be written as

$$\mathbf{k} = k_x\hat{e}_x + k_y\hat{e}_y + k_z\hat{e}_z \equiv k(l_x\hat{e}_x + l_y\hat{e}_y + l_z\hat{e}_z), \tag{B36}$$

where

$$l_x = \frac{k_x}{k}, \quad l_y = \frac{k_y}{k,} \quad l_z = \frac{k_z}{k} \tag{B37}$$

are the direction cosines of the complex wavenumber direction. In general, these are complex quantities but for homogeneous waves they are real and correspond also to the direction cosines of the propagation direction $\hat{\kappa} = \vec{\kappa}/|\vec{\kappa}|$ . For this kind of wave planes of constant phase (planes normal to the propagation vector $\hat{\kappa}$) are parallel to planes of constant amplitude (defined by $\vec{\alpha}\cdot\mathbf{x} = const.$).
Substitution of (B34) in the equation of motion (B33) yields the so called Christoffel equation,

$$(k^2\underset{\sim}{\Gamma} - \rho\omega^2\underset{\sim}{\mathbf{I}})\mathbf{U} = 0, \tag{B38}$$

where $\underset{\sim}{\mathbf{I}}$ is the identity matrix, and the Christofell matrix is defined by the following components:

$$\Gamma_{11} = p_{11}l_x^2 + p_{66}l_y^2 + p_{55}l_z^2 + 2p_{56}l_yl_z + 2p_{15}l_zl_x + 2p_{16}l_xl_y, \tag{B39a}$$

$$\Gamma_{22} = p_{66}l_x^2 + p_{22}l_y^2 + p_{44}l_z^2 + 2p_{24}l_yl_z + 2p_{46}l_zl_x + 2p_{26}l_xl_y, \tag{B39b}$$

$$\Gamma_{33} = p_{55}l_x^2 + p_{44}l_y^2 + p_{33}l_z^2 + 2p_{34}l_yl_z + 2p_{35}l_zl_x + 2p_{45}l_xl_y, \tag{B39c}$$

$$\Gamma_{12} = p_{16}l_x^2 + p_{26}l_y^2 + p_{45}l_z^2 + (p_{46} + p_{25})l_yl_z + (p_{14} + p_{56})l_zl_x + (p_{12} + p_{66})l_xl_y, \tag{B39d}$$

$$\Gamma_{13} = p_{15}l_x^2 + p_{46}l_y^2 + p_{35}l_z^2 + (p_{45} + p_{36})l_yl_z + (p_{13} + p_{55})l_zl_x + (p_{14} + p_{56})l_xl_y, \tag{B39e}$$

and

$$\Gamma_{23} = p_{56}l_x^2 + p_{24}l_y^2 + p_{34}l_z^2 + (p_{44} + p_{23})l_yl_z + (p_{36} + p_{45})l_zl_x + (p_{25} + p_{46})l_xl_y, \tag{B39f}$$

The dispersion relation for the AV solid is obtained by setting the characteristic determinant of (B38) equal to zero,

$$\Omega(\omega, k_x, k_y, k_z) = \det[k^2\underline{\Gamma} - \rho\omega^2\underline{\mathbf{I}}] = 0, \tag{B40}$$

Expansion of the determinant gives the complex dispersion relation

$$(\Gamma_{11}k^2 - \rho\omega^2)(\Gamma_{22}k^2 - \rho\omega^2)(\Gamma_{33}k^2 - \rho\omega^2) =$$

$$k^4[(\Gamma_{11}\Gamma_{23}^2 + \Gamma_{22}\Gamma_{13}^2 + \Gamma_{33}\Gamma_{12}^2)k^2 - \rho\omega^2(\Gamma_{12}^2 + \Gamma_{23}^2 + \Gamma_{13}^2)]. \tag{B41}$$

Equation (B41) defines a surface in $\kappa$-space, $\kappa = Re[k]$ as a function of the direction cosines. This is called the wavenumber surface. Unlike the AE case, here the Christoffel components are complex and frequency dependent as can be seen in equations (B39a-f).

## Complex and phase velocities

For simplicity, wave propagation in the $(x, z)$-plane ($l_y = 0$) of a TIV medium is considered, which due to the existence of a pure shear mode will be useful to clarify some concepts. Thus, only the stiffnesses $p_{11} = p_{22}$, $p_{33}$, $p_{44} = p_{55}$, $p_{12}$, $p_{13} = p_{23}$, and $p_{66} = (p_{11} - p_{12})/2$ , are different from zero. The Christoffel components (B39a-f) reduce to

$$\Gamma_{11} = p_{11}l_x^2 + p_{55}l_z^2, \tag{B42a}$$

$$\Gamma_{22} = p_{66}l_x^2 + p_{55}l_z^2, \tag{B42b}$$

$$\Gamma_{33} = p_{55}l_x^2 + p_{33}l_z^2, \tag{B42c}$$

$$\Gamma_{12} = \Gamma_{23} = 0, \tag{B42d}$$

and

$$\Gamma_{13} = (p_{13} + p_{55})l_zl_x, \tag{B42e}$$

and the dispersion relation (B41) separates into a linear factor

$$\Omega(\omega, k_x, k_z) = k^2\Gamma_{22} - \rho\omega^2 = 0, \tag{B43a}$$

and a quadratic factor

$$\Omega(\omega, k_x, k_z) = (k^2\Gamma_{11} - \rho\omega^2)(k^2\Gamma_{33} - \rho\omega^2) - k^4\Gamma_{13}^2 = 0, \tag{B43b}$$

or

$$\Gamma_{22} - \rho V_3^2 = 0, \tag{B44a}$$

and

$$(\Gamma_{11} - \rho V_m^2)(\Gamma_{33} - \rho V_m^2) - \Gamma_{13}^2 = 0, \quad m = 1,2 \tag{B44b}$$

respectively, where

$$V_m = \frac{\omega}{k_m}, \quad m = 1,...,3 \tag{B45}$$

are the complex velocities of the three modes, $qP$, $qSV$, and $SH$ respectively. The letter $q$ denotes "quasi". The last mode is uncoupled from the first two, with particle motion normal to the $(x, z)$-plane, and therefore is a pure propagating mode. Solving (B44a-b) for the complex velocity and replacing the Christoffel components (B42a-e) gives

$$V_1 = (2\rho)^{-\frac{1}{2}}(p_{55} + p_{11}l_x^2 + p_{33}l_z^2 + E)^{\frac{1}{2}}, \tag{B46a}$$

$$V_2 = (2\rho)^{-\frac{1}{2}}(p_{55} + p_{11}l_x^2 + p_{33}l_z^2 - E)^{\frac{1}{2}}, \tag{B46b}$$

and

$$V_3 = (2\rho)^{-\frac{1}{2}}(p_{66}l_x^2 + p_{55}l_z^2)^{\frac{1}{2}}, \tag{B46c}$$

with

$$E = \{[(p_{55} - p_{11})l_x^2 + (p_{33} - p_{55})l_z^2]^2 + 4(p_{13} + p_{55})^2 l_x^2 l_z^2\}^{\frac{1}{2}},$$

where $l_x$ and $l_z$ are given in equation (B37).
The phase velocity is defined as the frequency divided by the real wavenumber,

$$\mathbf{c}_m = \frac{\omega}{\kappa_m}\hat{\kappa} = \frac{\omega}{Re[k_m]}\hat{\kappa} = Re^{-1}\left[\frac{1}{V_m}\right]\hat{\kappa}, \tag{B47}$$

in virtue of equation (B45), where

$$\hat{\kappa} = \hat{e}_x l_x + \hat{e}_z l_z \tag{B48}$$

defines the propagation direction.
Equation (B47) represents the phase velocity for homogeneous plane waves in the $(x, z)$-plane. When $\omega \rightarrow 0$ the phase velocity gives the relaxed or elastic velocities $\mathbf{c}_{Rm}$ since $M_\nu \rightarrow 1$, $\nu = 1,2$ in equation (B8), and $p_{IJ} \rightarrow c_{IJ}$ by Condition 3. When $\omega \rightarrow \infty$, the phase velocities approach the unrelaxed velocities $\mathbf{c}_{um}$, which are obtained by replacing $M_\nu$ by its high-frequency limit $M_{u\nu}$ in the complex stiffness components $p_{IJ}$, where

$$M_{u\nu} = 1 - \sum_{l=1}^{L_\nu}\left(1 - \frac{\tau_{\epsilon l}^{(\nu)}}{\tau_{\sigma l}^{(\nu)}}\right), \quad \nu = 1,2 \tag{B49}$$

The examples consider two transversely-isotropic real earth materials: Mesaverde clayshale and Mesaverde calcareous sandstone. The elasticities are obtained in terms of the compressional and shear velocities $\alpha_0$, $\beta_0$ respectively, density $\rho$, and anisotropies $\varepsilon$, $\delta$ and $\gamma$ from the experimental data published by Thomsen (1986). They are given in Table 1 together with the set of relaxation times which define the anelastic properties of the medium. Relaxation times with superscript $\nu = 1$ represent anelastic processes which affect compressional motion; similarly $\nu = 2$ is related to the shear motion. In both cases there are two different mechanisms (i.e., $L_1 = L_2 = 2$). The elasticities are chosen as the relaxed components of the relaxation matrix. The complex stiffnesses are calculated according to equations (B11a-f). It can be verified that they satisfy the physical realizability conditions (B24a-c).
Figures B1 and B2 illustrate the phase velocity curves for TIV clayshale and sandstone respectively with (a) relaxed ($\omega = 0$), (b) $f = \omega/2\pi = 20Hz$, and (c) unrelaxed ($\omega = \infty$). There is a greater difference between the relaxed and unrelaxed phase velocities for the clayshale than for the sandstone. This is due to the fact that the clayshale relaxation times give more attenuation and velocity dispersion than the sandstone relaxation times. The inflexion points present in the $qSV$ mode of the clayshale are less pronounced for high frequencies. This affects the group and energy velocity curves since the inflexion points give rise to lacunas or cusps in these curves.

## Group velocity

The group velocity is the velocity of the modulation envelope of the wavefield, and as in the elastic case can be expressed by

$$\mathbf{c}_g = \hat{e}_x\frac{\partial\omega}{\partial\kappa_x} + \hat{e}_y\frac{\partial\omega}{\partial\kappa_y} + \hat{e}_z\frac{\partial\omega}{\partial\kappa_z}, \tag{B50}$$

where here the partial derivatives are taken with respect to the real wavenumber. Since there is not an explicit relation of the form $\omega = \Omega^R(\kappa_x, \kappa_y, \kappa_z)$, equation (B50) is not convenient. Alternatively, the group velocity can be obtained by implicit differentiation of the dispersion relations (43a-b). For instance

$$\frac{\partial\omega}{\partial\kappa_x} = \left[\frac{\partial\kappa_x}{\partial\omega}\right]^{-1} \tag{B51}$$

or since $\kappa_x = Re[k_x]$,

$$\frac{\partial\omega}{\partial\kappa_x} = Re^{-1}\left[\frac{\partial\kappa_x}{\partial\omega}\right] \tag{B52}$$

By implicit differentiation

$$\left(\frac{\partial\Omega}{\partial\omega}\delta\omega + \frac{\partial\Omega}{\partial k_x}\delta k_x\right)_{k_y,\,k_z} = 0, \tag{B53}$$

or

$$\left(\frac{\partial k_x}{\partial\omega}\right)_{k_y,\,k_z} = -\frac{\partial\Omega/\partial\omega}{\partial\Omega/\partial k_x}, \tag{B54}$$

and similar relations hold for the $k_y$ and $k_z$ components. Replacing the partial derivatives in (B50), the group velocity can be evaluated as

$$\mathbf{c}_g = -\left\{\hat{e}_x Re^{-1}\left[\frac{\partial\Omega/\partial\omega}{\partial\Omega/\partial k_x}\right] + \hat{e}_y Re^{-1}\left[\frac{\partial\Omega/\partial\omega}{\partial\Omega/\partial k_y}\right] + \hat{e}_z Re^{-1}\left[\frac{\partial\Omega/\partial\omega}{\partial\Omega/\partial k_z}\right]\right\}, \tag{B55}$$

For a TIV medium the dispersion relations (43a-b) may be expressed as

$$\Omega_3 = p_{66}k_x^2 + p_{55}k_z^2 - \rho\omega^2 = 0, \tag{B56a}$$

for the $SH$ mode, and

$$\Omega_m = (p_{11}k_x^2 + p_{55}k_z^2 - \rho\omega^2)(p_{55}k_x^2 + p_{33}k_z^2 - \rho\omega^2) - (p_{13} + p_{55})^2k_x^2k_z^2 = 0, \quad m = 1,2 \tag{B56b}$$

for the $qP$ and $qSV$ modes respectively, where equations (B37) and (B42a-e) have been used.
For instance, for the $SH$ mode the partial derivatives are

$$\frac{\partial\Omega_3}{\partial k_x} = 2p_{66}k_x, \tag{B57a}$$

$$\frac{\partial\Omega_3}{\partial k_z} = 2p_{55}k_z, \tag{B57b}$$

and

$$\frac{\partial\Omega_3}{\partial\omega} = p'_{66}k_x^2 + p'_{55}k_z^2 - 2\rho\omega, \tag{B57c}$$

where the prime denotes derivation with respect to the angular frequency. From equation (B10),

$$p'_{66} = c_{66}M'_2, \quad p'_{55} = c_{55}M'_2, \tag{B58a}$$

with

$$M'_2 = \sum_{l=1}^{L_\nu}\frac{i(\tau_{\epsilon l}^{(\nu)} - \tau_{\sigma l}^{(\nu)})}{(1 + \omega\tau_{\sigma l}^{(\nu)})^2}, \tag{B59}$$

Consequently, the group velocity for the $SH$ mode is obtained by substitution of equations (B57a-c) in (B55),

$$\vec{c}_{g3} = -2\left\{\hat{e}_x l_x Re^{-1}\left[\frac{D_3^g}{V_3 p_{66}}\right] + \hat{e}_z l_z Re^{-1}\left[\frac{D_3^g}{V_3 p_{55}}\right]\right\}, \tag{B60}$$

where

$$D_3^g = \omega(p'_{66}l_x^2 + p'_{55}l_z^2) - 2\rho V_3^2 = \omega\Gamma'_{22} - 2\rho V_3^2,$$

in terms of the complex velocity (B46c), Christoffel component (B42b) and direction cosines (B37).
Following the same procedure the group velocities for the $qP$ and $qSV$ modes are obtained:

$$c_{gm})_x = -2l_x Re^{-1}\left\{\frac{D_m^g}{V_m}[p_{11}w_m + p_{55}v_m - (p_{13} + p_{55})^2 l_z^2]^{-1}\right\}, \quad m = 1,2 \tag{B61a}$$

$$c_{gm})_z = -2l_z Re^{-1}\left\{\frac{D_m^g}{V_m}[p_{55}w_m + p_{33}v_m - (p_{13} + p_{55})^2 l_x^2]^{-1}\right\}, \quad m = 1,2 \tag{B61b}$$

where

$$D^g_m = (\omega\Gamma'_{11} - 2\rho V^2_m)w_m + (\omega\Gamma'_{33} - 2\rho V^2_m)v_m - 2\omega\Gamma_{13}\Gamma'_{13},$$

with

$$v_m = \Gamma_{11} - \rho V^2_m \tag{B62a}$$

and

$$w_m = \Gamma_{33} - \rho V^2_m \tag{B62b}$$

and in terms of the Christoffel components (B42a-e) and complex velocities (B46a-b).

Unlike the AE case, the group velocity is not equal to the wave surface velocity since, as shown in the following section, it is different from the energy velocity. The group velocity direction is normal to the phase velocity surface. This results from the fact that this surface is the representation of a real dispersion relation $\Omega^R(\omega, \kappa_x, \kappa_y, \kappa_z) = 0$, and that the group velocity can be expressed, by following the same calculations to obtain equation (B55), as proportional to the gradient of $\Omega^R$ with respect to $\vec{\kappa}$

In the IV limit the group velocity direction must be equal to the propagation direction. The *SH* mode is chosen for simplicity. For $p_{55} \to \mu$ and $p_{66} \to \mu$, equation (B60) reduces to

$$\mathbf{c}_{g3} = \hat{\kappa} Re^{-1}\left[\left(\frac{\rho}{\mu}\right)^{\frac{1}{2}}\left(1 - \frac{\omega}{2}\frac{\mu'}{\mu}\right)\right], \tag{B63}$$

where $\hat{\kappa}$ is defined in equation (B48), and

$$\mu' = \mu^e M'_2.$$

Equation (B63) was given in Carcione et al., (1988c). The same considerations hold for the other propagating modes, for which $\mathbf{c}_{g1}$ is obtained by replacing $\mu$ by $\lambda + 2\mu$ in equation (B63), and $\mathbf{c}_{g2} = \mathbf{c}_{g3}$

The group velocity curves for TIV clayshale are shown in Figure B3 with (a) relaxed, (b) $f = 20Hz$, and (c) unrelaxed. The $qSV$ velocity presents singularities at the turning points of the cusps for finite values of the frequency. Since the physical realizability conditions are satisfied for any frequency, this would mean that the concept of group velocity has no physical meaning at the cusps. These singularities are not present in the other two propagating modes. It is known that for low $Q$ materials the group velocity loses its physical meaning since the strong velocity dispersion spreads the wave packet significantly. Figure B4 shows the group velocity for TIV sandstone at $f = 20Hz$

## Energy velocity

The energy velocity is defined as the ratio of the average power flow density to the mean energy density. The average power flow density is the real part of the complex Poynting vector, hence

$$\mathbf{c}_e = \frac{Re[\mathbf{p}]}{\varepsilon_{AV}}, \tag{B64}$$

or substituting equation (B21),

$$\mathbf{c}_e = \frac{2Re[\mathbf{p}]}{(\varepsilon_v)_{peak} + (\varepsilon_s)_{peak}}, \tag{B65}$$

The Poynting vector is calculated in first place, considering a plane wave polarized in the $(x, z)$-plane with particle displacement components

$$u_x = U_x e^{i(\omega t - k_x x - k_z z)}, \tag{B66a}$$

and

$$u_z = U_z e^{i(\omega t - k_x x - k_z z)}, \tag{B66b}$$

with

$$\mathbf{k} = k_x\hat{e}_x + k_z\hat{e}_z = (\kappa - i\alpha)\hat{\kappa}, \tag{B67}$$

i.e., a homogeneous plane wave.

The associated strain components are

$$S_1 = \frac{\partial u_x}{\partial x} = -ik_x U_x e^{i(\omega t - \mathbf{k}\cdot\mathbf{x})}, \tag{B68a}$$

$$S_3 = \frac{\partial u_z}{\partial z} = -ik_z U_z e^{i(\omega t - \mathbf{k}\cdot\mathbf{x})}, \tag{B68b}$$

and

$$S_5 = \frac{\partial u_x}{\partial z} + \frac{\partial u_z}{\partial x} = -i(k_z U_x + k_x U_z)e^{i(\omega t - \mathbf{k}\cdot\mathbf{x})}, \qquad (B68c)$$

For a TIV medium the stress components are

$$T_1 = p_{11}S_1 + p_{13}S_3 = -i(p_{11}k_x U_x + p_{13}k_z U_z)e^{-\vec{\alpha}\cdot\mathbf{x}}e^{i(\omega t - \vec{\kappa}\cdot\mathbf{x})}, \qquad (B69a)$$

$$T_3 = p_{13}S_1 + p_{33}S_3 = -i(p_{13}k_x U_x + p_{33}k_z U_z)e^{-\vec{\alpha}\cdot\mathbf{x}}e^{i(\omega t - \vec{\kappa}\cdot\mathbf{x})}, \qquad (B69b)$$

and

$$T_5 = p_{55}S_5 = -ip_{55}(k_z U_x + k_x U_z)e^{-\vec{\alpha}\cdot\mathbf{x}}e^{i(\omega t - \vec{\kappa}\cdot\mathbf{x})}, \qquad (B69c)$$

From (B15) the complex Poynting vector is

$$\mathbf{p} = -\frac{1}{2}[\hat{e}_x(\dot{u}_x^* T_1 + \dot{u}_z^* T_5) + \hat{e}_z(\dot{u}_x^* T_5 + \dot{u}_z^* T_3)]. \qquad (B70)$$

Replacing (B68a-c) in (B69a-c) and the results in (B70) yields

$$p_x = \frac{1}{2}\omega k_m e^{-2\vec{\alpha}_m\cdot\mathbf{x}}[p_{11}l_x|U_x|^2 + p_{13}U_x^* U_z l_z + p_{55}(U_x U_z^* l_z + |U_z|^2 l_x)], \qquad (B71a)$$

$$p_z = \frac{1}{2}\omega k_m e^{-2\vec{\alpha}_m\cdot\mathbf{x}}[p_{33}l_z|U_z|^2 + p_{13}U_z^* U_x l_x + p_{55}(U_z U_x^* l_x + |U_x|^2 l_z)], \qquad (B71b)$$

where equation (B37) has been used. In equations (B71a-b) $m = 1$ identifies the $qP$ mode and $m = 2$ the $qSV$ mode. The ratio $U_x$ to $U_z$ is obtained by substitution of (B71a-b) in the Christoffel equation (B38). For instance, from the first line,

$$B_m \equiv \frac{U_z}{U_x} = -\frac{k_m^2\Gamma_{11} - \rho\omega^2}{k_m^2\Gamma_{13}} = -\frac{\Gamma_{11} - \rho V_m^2}{\Gamma_{13}}, \quad m = 1,2 \qquad (B72a)$$

and from the third line,

$$B_m = -\frac{\Gamma_{13}}{\Gamma_{33} - \rho V_m^2}, \quad m = 1,2 \qquad (B72b)$$

according to equation (B45). Replacing $B_m$ the Poynting vector components (71a-b) become

$$p_x = \frac{1}{2}\omega k_m e^{-2\vec{\alpha}_m\cdot\mathbf{x}}|U_x|^2[p_{11}l_x + p_{13}B_m l_z + p_{55}(B_m^* l_z + |B_m|^2 l_x)], \qquad (B73a)$$

$$p_z = \frac{1}{2}\omega k_m e^{-2\vec{\alpha}_m\cdot\mathbf{x}}|U_x|^2[p_{55}(l_z + B_m l_x) + p_{13}B_m^* l_x + p_{33}|B_m|^2 l_z]. \qquad (B73b)$$

The peak kinetic energy density is from (B20) and (B66a-b),

$$(\varepsilon_V)_{peak} = \frac{1}{2}\rho\omega^2|U_x|^2 e^{-2\vec{\alpha}_m\cdot\mathbf{x}}(1 + |B_m|^2). \qquad (B74)$$

The peak potential energy density is from equation (B19),

$$(\varepsilon_s)_{peak} = \frac{1}{2}[S_1(r_{11}S_1^* + r_{13}S_3^*) + S_3(r_{13}S_1^* + r_{33}S_3^*) + r_{55}|S_5|^2]. \qquad (B75)$$

After substitution of the strain components (B68a-c) and equation (B72a-b) the potential energy density becomes

$$(\varepsilon_s)_{peak} = \frac{1}{2}|k_m|^2|U_x|^2 e^{-2\vec{\alpha}_m\cdot\mathbf{x}}[l_x^2 r_{11} + l_z^2 r_{55} + B_m B_m^*(l_x^2 r_{55} + l_z^2 r_{33}) + (r_{13} + r_{55})l_x l_z(B_m + B_m^*)], \qquad (B76)$$

or using (B5a) and replacing the Christoffel components (B42a-e),

$$(\varepsilon_s)_{peak} = \frac{1}{2}|k_m|^2|U_x|^2 e^{-2\vec{\alpha}_m\cdot\mathbf{x}}Re[\Gamma_{11} + B_m B_m^*\Gamma_{33} + (B_m + B_m^*\Gamma_{13}], \qquad (B77)$$

which in virtue of equations (B72a-b) reduces to

$$(\varepsilon_s)_{peak} = \frac{1}{2}\rho|k_m|^2|U_x|^2 e^{-2\vec{\alpha}_m\cdot\mathbf{x}}(1 + |B_m|^2)Re[V_m^2]. \qquad (B78)$$

In consequence, the sum of the peak kinetic and potential energy densities gives

$$(\varepsilon_v)_{peak} + (\varepsilon_s)_{peak} = \frac{1}{2}\rho\omega^2|U_x|^2(1 + |B_m|^2)e^{-2\vec{\alpha}_m\cdot\mathbf{x}}\{1 + |V_m^{-1}|^2 Re[V_m^2]\}, \tag{B79}$$

by equation (B45). Using the following properties of complex numbers,

$$|z^{-1}|^2 = |z^2|^{-1}, \quad Re[z^{-1}] = |z^2|^{-1}Re[z], \tag{B80a}$$

and

$$Re^2[z] = \frac{|z^2| + Re[z^2]}{2}, \tag{B80b}$$

equation (B79) becomes

$$(\varepsilon_v)_{peak} + (\varepsilon_s)_{peak} = \rho\omega^2|U_x|^2(1 + |B_m|^2)e^{-2\vec{\alpha}_m\cdot\mathbf{x}}Re[V_m]Re[V_m^{-1}]. \tag{B81}$$

Finally replacing (B73a-b) and (B81) in equation (B65) gives the energy velocity for the $qP$ and $qSV$ modes,

$$c_{em})_x = c_m(D_m^e)^{-1}Re\{V_m^{-1}[p_{11}l_x + p_{13}B_m l_z + p_{55}(B_m^* l_z + |B_m|^2 l_x)]\}, \quad m = 1,2 \tag{B82a}$$

$$c_{em})_z = c_m(D_m^e)^{-1}Re\{V_m^{-1}[p_{55}(l_z + B_m l_x) + p_{13}B_m^* l_x + p_{33}|B_m|^2 l_z)]\}, \quad m = 1,2 \tag{B82b}$$

where

$$D_m^e = \rho(1 + |B_m|^2)Re[V_m],$$

with the use of equation (B47).

Special care has to be taken for a numerical evaluation of equations (B82a-b) when either $l_x$ or $l_z \to 0$. For instance when $l_x \to 0$ and $l_z \to 1$, $B_1 \to \infty$ and $B_2 \to 0$. Taking these limits give the appropiate formulae as is shown in a following section.

Similarly, the energy velocity for the $SH$ mode ($m = 3$) is calculated. In this case the wave is polarized normal to the $(x, z)$-plane, and therefore normal to the propagation direction. Only the strains $S_4$ and $S_6$ are different from zero. The calculation is much more simple than before and the energy velocity can be written as

$$\mathbf{c}_{e3} = c_3\rho^{-1}Re^{-1}[V_3]Re\{V_3^{-1}[\hat{e}_x l_x p_{66} + \hat{e}_z l_z p_{55}]\}. \tag{B83}$$

An alternative approach to compute the energy velocity is to find the locus of the points $(x/t, z/t)$ which makes the phase equal to zero (Postma , 1955):

$$\omega t - \kappa_m(x l_x + z l_z) = 0. \tag{B84}$$

Replacing the phase velocity (B47) and defining

$$\theta = \sin^{-1} l_x, \tag{B85}$$

equation (B84) gives

$$c_m = \left(\frac{x}{t}\right)\sin\theta + \left(\frac{z}{t}\right)\cos\theta. \tag{B86}$$

Taking derivatives with respect to the angle yields

$$\frac{dc_m}{d\theta} = \left(\frac{x}{t}\right)\cos\theta - \left(\frac{z}{t}\right)\sin\theta. \tag{B87}$$

Squaring equation (B86) and adding the result to (B87) gives

$$c_{em}[\varphi(\theta)] = \left[\left(\frac{x}{t}\right)^2 + \left(\frac{z}{t}\right)^2\right]^{\frac{1}{2}} = \left[c_m^2(\theta) + \left(\frac{dc_m}{d\theta}\right)^2\right]^{\frac{1}{2}}. \tag{B88}$$

The energy velocity direction is given by

$$\varphi(\theta) = \tan^{-1}\left(\frac{x/t}{z/t}\right) = \theta - \tan^{-1}\left(\frac{dc_m/d\theta}{c_m}\right). \tag{B89}$$

Equation (B88) is the well known expression of the group velocity in TIE media (Berryman, 1979), not valid in this sense for TIV media.

Note that equation (B84) express an important relation between the phase and energy velocities:

$$\hat{\kappa}\cdot\mathbf{c}_{em} = c_m, \tag{B90}$$

demonstrated by Auld (1973, p. 222) for AE media. In the case of a TIV medium this relation is easily verified for $SH$ waves by taking the dot product of the $SH$ energy velocity (B83) and the propagation direction vector (B48), while for the $qP$ and $qSH$ modes it can be obtained by also using equations (B72a-b) and (B42a-e). Since the wave surface is the envelope of plane waves with wavenumber vector $\vec{\kappa}$, this is normal to the wavefront at point $\mathbf{x}$ . This also results from the fact that $dc/d\theta$ defined by equation (B87) is tangent to the wavefront at point $\mathbf{x}$ . Similarly to the AE case the energy velocity direction (or the position vector direction) is normal to the phase velocity surface. This is shown in the following demonstration:

**Geometrical relation between the phase velocity surface and energy velocity direction:** To prove that the energy velocity vector is normal to the phase velocity surface the demonstration follows a similar procedure described by Auld (1973, p 226) for AE media. Consider two plane waves having infinitesimally different directions of propagation and the same frequency. Then

$$\frac{\vec{\kappa}'}{\omega} = \frac{\vec{\kappa} + \delta\vec{\kappa}}{\omega}, \quad \mathbf{c}'_e = \mathbf{c}_e + \delta\mathbf{c}_e. \tag{B91}$$

Applying (B90) to the wavenumber vector $\vec{\kappa}'$ gives

$$\frac{\hat{\kappa}' \cdot \mathbf{c}'_e}{\mathbf{c}'} = \frac{\vec{\kappa}'}{\omega} \cdot \mathbf{c}'_e = 1, \tag{B92}$$

or

$$\left(\frac{\vec{\kappa} + \delta\vec{\kappa}}{\omega}\right) \cdot (\mathbf{c}_e + \delta\mathbf{c}_e) = \frac{\vec{\kappa} \cdot \mathbf{c}_e}{\omega} + \frac{\delta\vec{\kappa} \cdot \mathbf{c}_e}{\omega} + \frac{\vec{\kappa} \cdot \delta\mathbf{c}_e}{\omega} = 1, \tag{B93}$$

where second order terms have been ignored. Using again (B90), (B93) results in

$$\frac{\delta\vec{\kappa} \cdot \mathbf{c}_e}{\omega} + \frac{\vec{\kappa} \cdot \delta\mathbf{c}_e}{\omega} = 0. \tag{B94}$$

But since the wavenumber vector $\vec{\kappa}$ is normal to the wave surface, and $\delta\mathbf{c}_e$ always lie on this surface,

$$\frac{\vec{\kappa} \cdot \delta\mathbf{c}_e}{\omega} = 0, \tag{B95}$$

which means that

$$\frac{\delta\vec{\kappa} \cdot \mathbf{c}_e}{\omega} = 0. \tag{B96}$$

Since $\delta\vec{\kappa}$ is tangent to the phase velocity surface, $\mathbf{c}_e$ is normal to this surface. A more rigorous demonstration of obtaining equation (B96) for AE media is given by Auld (1973, p. 225, eq. (7.71)). The procedure can be generalized to AV media obtaining

$$\delta\mathbf{k} \cdot \mathbf{p} = 0. \tag{B97}$$

For homogeneous waves, i.e., the directions of the complex and real wavenumbers coincide, equation (B97) is equivalent to (B96) considering the definition of energy velocity (B64).

In the IV limit, equations (B82a-b) and (B83) must give the phase velocity (Borcherdt, 1973). For instance, for the $SH$ mode in the limit $p_{66} \rightarrow \mu$ and $p_{55} \rightarrow \mu$ the complex velocity is from (B46c), $V_3 = (\mu/\rho)^{1/2}$. Therefore equation (B83) becomes

$$\mathbf{c}_{e3} = \hat{\kappa} c_3 = \hat{\kappa} Re^{-1}\left[\left(\frac{\rho}{\mu}\right)^{\frac{1}{2}}\right], \tag{B98}$$

i.e., the shear phase velocity in an IV medium (Carcione et al., 1988c). In the IV limit, $p_{11} = p_{33} = \lambda + 2\mu$, $p_{13} = \lambda$, and $p_{55} = \mu$, therefore $B_m$ in equation (B72a) reduces to

$$B_1 = \frac{l_z}{l_x} \tag{B99a}$$

for $P$ waves, and

$$B_2 = -\frac{l_x}{l_z} \tag{B99b}$$

for $S$ waves. Replacing these values in equations (B82a-b) the energy velocity becomes the phase velocity. In the AE limit, $p_{55} \rightarrow r_{55} \rightarrow c_{55}$, and $p_{66} \rightarrow r_{66} \rightarrow c_{66}$. A short calculation shows that in this limit the group and energy velocities for the $SH$ mode (equations (B60) and (B83) respectively) are identical, a condition that is

also valid for the coupled modes (see Auld, 1973, p. 279). This is equivalent to saying that the relaxed group and energy velocities coincide. It may be seen that when $\omega \to \infty$ the unrelaxed velocities are also identical.
The energy velocity curves for TIV clayshale and sandstone are given in Figures B5 and B6 respectively with (a) relaxed, (b) $f = 20Hz$, (c) unrelaxed. The curves represent sections of the wavefront. The relaxed curves correspond to the AE wavefronts and are identical to the group velocity curves represented in Figure B3a (clayshale). Unrelaxed group and energy velocities also coincide (see Figures B4c and B6c respectively). Actually, when $\omega \to \infty$ the material behavior is elastic as is shown by the representations of the quality factors versus frequency ($Q \to \infty$) in the following section. Since the elastic limit was chosen when $\omega \to 0$, a wave travelling in an AV material is faster than a wave in the corresponding AE material. Conversely it is possible to choose the elastic behavior in the high-frequency limit (see Ben-Menahem and Singh, 1981, p. 873). In this case a wave travelling in an AV solid has lower velocity than a wave in the corresponding AE medium.
At intermediate frequencies the group velocity is greater than the energy velocity (compare Figures B3b and B5b for clayshale, and B4b and B6b for sandstone). For pure mode directions, for instance, the symmetry axis and the direction normal to it, the phase velocity and the energy velocity coincide for all the frequencies.

## Quality factors

The quality factor is defined as the ratio of the peak strain energy density (B19) to the loss in energy density due to anelasticity (B22). Then

$$Q = \frac{(\varepsilon_s)_{peak}}{(\varepsilon_d)_{AV}} = \frac{\mathbf{S}:\underset{\sim}{\mathbf{R}}:\mathbf{S}^*}{\mathbf{S}:\underset{\sim}{\mathbf{Q}}:\mathbf{S}^*}. \qquad (B100)$$

The loss in energy density is calculated in a similar way to the strain energy density (B78), replacing $r_{IJ}$ by $q_{IJ}$. It gives

$$(\varepsilon_v)_{AV} = \frac{1}{2}\rho|k_m|^2|U_x|^2 e^{-2\vec{\alpha}_m\cdot\mathbf{x}}(1 + |B_m|^2)Im[V_m^2]. \qquad (B101)$$

Then the quality factors for the $qP$ and $qSV$ modes are

$$Q_m = \frac{Re[V_m^2]}{Im[V_m^2]} \quad m = 1,2 \qquad (B102a)$$

Similarly for the $SH$ mode,

$$Q_3 = \frac{Re[V_3^2]}{Im[V_3^2]} \qquad (B102b)$$

Using equation (B45) and basic properties of complex numbers, the quality factors can be expressed as

$$Q_m = -\frac{Re[k_m^2]}{Im[k_m^2]} \quad m = 1,3 \qquad (B103)$$

This is the well known equation found for homogeneous waves in an IV medium (Borcherdt, 1973), which is still valid in a TIV medium.
In the IV limit, equations (B102a-b) and (B103) yield

$$Q_1 = \frac{Re[\lambda + 2\mu]}{Im[\lambda + 2\mu]} \qquad (B104a)$$

for $P$ waves, and

$$Q_2 = Q_3 = \frac{Re[\mu]}{Im[\mu]} \qquad (B104b)$$

for $S$ waves.
Figures B7 and B8 represent the quality factors

$$Q_x = Ql_x, \quad Q_z = Ql_z, \qquad (B105)$$

(for homogeneous waves the attenuation and propagation directions coincide) for TIV clayshale and sandstone respectively. As can be seen from Figures B1 and B2 the quality factor curves follow approximately the shape of the phase velocity curves (these effect is more pronounced in the $qSV$ mode). The $qSV$ mode in the clayshale has higher attenuation at $\theta = \pi/4$ than in the symmetry axis, while in the sandstone the opposite effect occurs. Since the symmetry axis is a pure mode direction, like the direction normal to it, $Q_2$ coincides with $Q_3$. In particular the $SH$ quality factor is isotropic, since replacing (B46c) in (B102b) and using (B10) gives $Q_3 = Re[M_2]/Im[M_2]$, i.e., independent of the propagation direction.

## Analysis in the symmetry axis of a TIV medium

The symmetry axis of a TIV medium represents a pure mode direction in the sense that the displacement vector is either parallel or normal to the real wavenumber $\vec{\kappa}$. In this direction the wave solutions become purely transverse and purely longitudinal like in an IV medium. In the symmetry axis is $l_x = 0$ and $l_z = 1$, and the phase velocities (B47) reduce to

$$c_1 = Re^{-1}\left[\left(\frac{\rho}{p_{33}}\right)^{\frac{1}{2}}\right], \tag{B106a}$$

and

$$c_2 = c_3 = Re^{-1}\left[\left(\frac{\rho}{p_{55}}\right)^{\frac{1}{2}}\right]. \tag{B106b}$$

Similarly replacing the complex velocities (B45a-b) in (B60) and (B61a-c), the group velocities become

$$c_{g1} = Re^{-1}\left[\left(\frac{\rho}{p_{33}}\right)^{\frac{1}{2}}\left(1 - \frac{\omega}{2}\frac{p'_{33}}{p_{33}}\right)\right], \tag{B107a}$$

and

$$c_{g2} = c_{g3} = Re^{-1}\left[\left(\frac{\rho}{p_{55}}\right)^{\frac{1}{2}}\left(1 - \frac{\omega}{2}\frac{p'_{55}}{p_{55}}\right)\right], \tag{B107b}$$

These results are analogous to the ones found for IV media (see equation (B63) and Carcione et al., 1988c). The energy velocity is obtained from equations (B82a-b) and (B83) with the use of (B72a). When $l_x \rightarrow 0$ and $l_z \rightarrow 1$, $B_1 \rightarrow \infty$, and $B_2 \rightarrow 0$. In this limit the energy velocity gives the phase velocity. This result is valid for any direction in IV media (Borcherdt, 1973).
Finally, the quality factors (102a-b) in the symmetry axis reduce to

$$Q_1 = \frac{Re[p_{33}]}{Im[p_{33}]}, \tag{B108a}$$

for the $qP$ mode, and

$$Q_2 = Q_3 = \frac{Re[p_{55}]}{Im[p_{55}]} = \frac{Re[M_2]}{Im[M_2]}, \tag{B108b}$$

for the shear modes. Figure B9 shows the phase and group velocities versus frequency for TIV clayshale in the symmetry axis with (a) $P$ wave, and (b) $S$ wave. As can be seen they coincide at the low and high-frequency limits. Relatively, the shear modes have more velocity dispersion than the longitudinal mode, 20 % and 18 % respectively. This is related to the fact that the shear quality factors are lower than the longitudinal quality factor as can be appreciated in Figure B10a. Since the kernels $M_v$ are analytic functions in the lower $\omega$-plane, the system's impulse response is real and causal, and therefore the Kramers-Kronig relations are valid (see Ben-Menahem and Singh, 1981, p. 916 and 1050). This is also a consequence of the causality principle which is inherent in Boltzmann's superposition principle.
For comparison, the quality factors in the symmetry axis and $\theta = \pi/4$ are represented in Figures (B10a-b) and (B11a-b) for clayshale and sandstone respectively. At $\theta = \pi/4$, the $qSV$ quality factor for sandstone is greater than the $qP$ quality factor (see also Figure B8). In particular, the set of relaxation times chosen for the two materials gives almost constant $Q$ values in the exploration seismic band.

## Comparison among the different rheologies

The comparison of the physical velocities and quality factors among the different rheologies can be summarized in the following:

**IE rheology**

$$\mathbf{c} = \mathbf{c}_e = \mathbf{c}_g, \tag{B109a}$$

$$Q_m = \infty. \tag{B109b}$$

Wavefronts are spherical. The energy flux direction coincides with the propagation direction and all the physical velocities are identical.

**IV rheology**

$$\mathbf{c} = \mathbf{c}_e \neq \mathbf{c}_g, \tag{B110a}$$

$$\mathbf{c}_R = \mathbf{c}_{eR} = \mathbf{c}_{gR}; \quad \mathbf{c}_u = \mathbf{c}_{eu} = \mathbf{c}_{gu}, \tag{B110b}$$

$$Q_1 = \frac{Re[\lambda + 2\mu]}{Im[\lambda + 2\mu]}, \quad Q_2 = Q_3 = \frac{Re[\mu]}{Im[\mu]}. \tag{B110c}$$

The subscripts $R$ and $u$ denote relaxed and unrelaxed respectively. Wavefronts are spherical and frequency dependent. The direction of the three physical velocities coincide but the group velocity differs in magnitude from the phase and energy velocities.

**AE rheology**

$$\mathbf{c} \neq \mathbf{c}_e = \mathbf{c}_g, \tag{B111a}$$

$$Q_m = \infty. \tag{B111b}$$

Wavefronts are not spherical. The energy flux does not coincide with the propagation direction. The energy velocity is the group velocity. The wavenumber vector is normal to the wave surface, and the energy velocity vector is normal to the phase velocity surface.

**AV rheology**

$$\mathbf{c} \neq \mathbf{c}_e \neq \mathbf{c}_g, \quad \mathbf{c} \neq \mathbf{c}_g, \tag{B112a}$$

$$\mathbf{c}_R \neq \mathbf{c}_{eR} = \mathbf{c}_{gR}; \quad \mathbf{c}_u \neq \mathbf{c}_{eu} = \mathbf{c}_{gu}, \tag{B112b}$$

$$Q_m = Q_m(l_x, l_y, l_z). \tag{B112c}$$

Generalizing the results obtained for TIV media, I conclude that as in the IV case, each frequency component has a different wavefront not spherical in this case. The physical velocities differ from each other in magnitude and direction. Quality factors and velocity dispersion are not isotropic. At least for propagation in the $(x, z)$ -plane of a TIV medium (the case considered in this section) the real wavenumber vector is normal to the wave surface and the velocity vector is normal to the phase velocity surface.

**Pure mode directions in an AV rheology**

$$\mathbf{c} = \mathbf{c}_e \neq \mathbf{c}_g, \tag{B113a}$$

$$\mathbf{c}_R = \mathbf{c}_{eR} = \mathbf{c}_{gR}; \quad \mathbf{c}_u = \mathbf{c}_{eu} = \mathbf{c}_{gu}, \tag{B113b}$$

$$Q_1 = \frac{Re[p_{33}]}{Im[p_{33}]}, \quad Q_2 = Q_3 = \frac{Re[p_{55}]}{Im[p_{55}]}, \tag{B113c}$$

for instance in the symmetry axis of a TIV medium. The situation is analogous to that of IV media.
When the propagation is in the $(x, y)$-plane the dispersion relation (B41) is independent of the propagation direction in the plane. There is one pure longitudinal mode, one pure shear mode polarized parallel to the $z$-axis, and another pure shear mode polarized normal to the $z$-axis, with complex velocities $V_1 = (p_{11}/\rho)^{1/2}$, $V_2 = (p_{55}/\rho)^{1/2}$ , and $V_3 = (p_{66}/\rho)^{1/2}$ respectively. In this case the shear waves are said to be birefingent because the velocities are different, and the complete set of modes is called trirefringent.

**2-D problem:** The same equations obtained for wave propagation in the $(x, z)$ -plane of the 3-D TIV medium are valid for the 2-D case. In the expressions of phase velocities (B47), group velocities (B60) and (B61a-b), energy velocities (B82a-b) and quality factors (B102a-b), the complex stiffnesses $p_{11}$, $p_{12}$, $p_{22}$ and $p_{33}$ of equation (B12) (2-D case), play the role of $p_{11}$, $p_{13}$, $p_{33}$ and $p_{55}$ respectively, of equation (B10) (3-D case).

## REFERENCES


Auld, B.A., 1973. Acoustic fields and waves in solids, Vol. 1, John Wiley & Sons, Inc., New York,

Ben-Menahem, A.B., & Singh, S.J., 1981. Seismic waves and sources, Springer Verlag, New York.

Berryman, J.G., 1979. Long-wave elastic anisotropy in transversely isotropic media, Geophysics, **44**, 896-917.

Borcherdt, R.D., 1973. Energy and plane waves in linear viscoelastic media, J. Geophys. Res., **78**, 2442-2453.

Carcione, J.M., Kosloff, D., & Kosloff, R., 1988c. Wave propagation simulation in a linear viscoelastic medium, Geophys. J. Roy. Astr. Soc., **95**, 597-611.

Korn, G.A., & Korn, T.M., 1961. Mathematical handbook for scientists and engineers, Mc Graw-Hill, New York.

Thomsen, L., 1986. Weak elastic anisotropy, Geophysics, **51**, 1954-1966.

# APPENDIX C

## ROTATION OF THE RELAXATION MATRIX

Frequently, to solve a wave propagation problem in anisotropic media it is necessary to transform the realaxtion matrix to another system of coordinates. For instance, a TIV medium is considered whose symmetry axis does not coincide with the $z'$-axis of the cartesian system $S'$ where the problem must be solved. Since the experimental elasticities are given in a system $S$ whose $z$ -axis coincides with the symmetry axis, a rotation of the relaxation matrix $\Psi$ from $S$ to $S'$ is necessary in order to obtain $\Psi'$.
As demonstrated by Auld (1973, p. 76) the transformation law is given by

$$\psi'_{IJ} = t_{IL} t_{JK} \psi_{LK}, \quad I,J,K,L = 1,\ldots,6 \tag{C1}$$

or in matrix notation

$$\underset{\sim}{\Psi}' = \underset{\sim}{\mathbf{T}}\underset{\sim}{\Psi}\underset{\sim}{\mathbf{T}}^T, \tag{C2}$$

where $\underset{\sim}{\mathbf{T}}$ is a 6 x 6 transformation matrix with components $t_{IJ}$ . $\underset{\sim}{\mathbf{T}}$ is given by (Auld, 1973, p. 74),

$$\underset{\sim}{\mathbf{T}} = \begin{bmatrix} a_{xx}^2 & a_{xy}^2 & a_{xz}^2 & 2a_{xy}a_{xz} & 2a_{xz}a_{xx} & 2a_{xx}a_{xy} \\ a_{yx}^2 & a_{yy}^2 & a_{yz}^2 & 2a_{yy}a_{yz} & 2a_{yz}a_{yx} & 2a_{yx}a_{yy} \\ a_{zx}^2 & a_{zy}^2 & a_{zz}^2 & 2a_{zy}a_{zz} & 2a_{zz}a_{zx} & 2a_{zx}a_{zy} \\ a_{yx}a_{zx} & a_{yy}a_{zy} & a_{yz}a_{zz} & a_{yy}a_{zz} + a_{yz}a_{zy} & a_{yx}a_{zz} + a_{yz}a_{zx} & a_{yy}a_{zx} + a_{yx}a_{zy} \\ a_{zx}a_{xx} & a_{zy}a_{xy} & a_{zz}a_{xz} & a_{xy}a_{zz} + a_{xz}a_{zy} & a_{xz}a_{zx} + a_{xx}a_{zz} & a_{xx}a_{zy} + a_{xy}a_{zx} \\ a_{xx}a_{yx} & a_{xy}a_{yy} & a_{xz}a_{yz} & a_{xy}a_{yz} + a_{xz}a_{yy} & a_{xz}a_{yx} + a_{xx}a_{yz} & a_{xx}a_{yy} + a_{xy}a_{yx} \end{bmatrix}, \tag{C3}$$

with $a_{ij}$ the direction cosine of the angle between the $x'_i$-axis an the $x_j$-axis.
The example illustrates a clockwise rotation of coordinates through an angle $\beta$ about the $y$-axis coincident with the $y'$-axis. Hence, the direction cosine matrix is

$$\underset{\sim}{\mathbf{A}} = \begin{bmatrix} a_{xx} & a_{xy} & a_{xz} \\ a_{yx} & a_{yy} & a_{yz} \\ a_{zx} & a_{zy} & a_{zz} \end{bmatrix} = \begin{bmatrix} \cos\beta & 0 & \sin\beta \\ 0 & 1 & 0 \\ -\sin\beta & 0 & \cos\beta \end{bmatrix}, \tag{C4}$$

and from (C3) the corresponding transformation matrix is

$$\underset{\sim}{\mathbf{T}} = \begin{bmatrix} \cos^2\beta & 0 & \sin^2\beta & 0 & \sin\beta & 0 \\ 0 & 1 & 0 & 0 & 0 & 0 \\ \sin^2\beta & 0 & \cos^2\beta & 0 & -\sin 2\beta & 0 \\ 0 & 0 & 0 & \cos\beta & 0 & -\sin\beta \\ -\dfrac{\sin 2\beta}{2} & 0 & \dfrac{\sin 2\beta}{2} & 0 & \cos 2\beta & 0 \\ 0 & 0 & 0 & \sin\beta & 0 & \cos\beta \end{bmatrix}. \tag{C5}$$

Any general rotation can be performed by applying successive rotations of the type (C5) about different coordinates axis.
An alternative method to equation (C2) is to apply the rotation to the elasticity matrix and then introduce the anelasticity. Of course these two different approaches do not give the same results.

## REFERENCES

Auld, B.A., 1973. Acoustic fields and waves in solids, Vol. 1, John Wiley & Sons, Inc., New York.

## APPENDIX D

## TWO-DIMENSIONAL EQUATIONS OF MOTION

For a TIV medium the rheological relation is given by equation (9), with $c_{15} = c_{35} = 0$. For $L_1 = L_2 = 1$, i.e. one relaxation mechanism for each mode, equation (21) becomes

$$T_1 = [(c_{11} - D) + (D - c_{55})M_{u1} + c_{55}M_{u2}]S_1 + [(c_{13} + 2c_{55} - D) + (D - c_{55})M_{u1} - c_{55}M_{u2}]S_3 + (D - c_{55})e_1 + c_{55}e_2, \qquad (D1a)$$

$$T_3 = [(c_{33} - D) + (D - c_{55})M_{u1} + c_{55}M_{u2}]S_3 + [(c_{13} + 2c_{55} - D) + (D - c_{55})M_{u1} - c_{55}M_{u2}]S_1 + (D - c_{55})e_1 - c_{55}e_2, \qquad (D1b)$$

and

$$T_5 = c_{55}M_{u2}S_5 + c_{55}e_3, \qquad (D1c)$$

where

$$e_1 \equiv e_{11}^{(1)} + e_{31}^{(1)} = \varphi_1{}^*(S_1 + S_3), \qquad (D2a)$$

$$e_2 \equiv e_{11}^{(2)} + e_{31}^{(2)} = \varphi_2{}^*(S_1 - S_3), \qquad (D2b)$$

and

$$e_3 = e_{51}^{(2)} = \varphi_2{}^*S_5, \qquad (D2c)$$

are combinations of the memory variables (20). In this example particularly there are the same number of unknown variables as in the 2-D IV case (Carcione et al., 1988c).
The equivalent expressions to equation (22) are

$$\dot{e}_1 = (S_1 + S_3)\varphi_1(0) - e_1/\tau_{\sigma l}^{(1)}, \qquad (D3a)$$

$$\dot{e}_2 = (S_1 - S_3)\varphi_2(0) - e_2/\tau_{\sigma l}^{(2)}, \qquad (D3b)$$

and

$$\dot{e}_3 = S_5\varphi_2(0) - e_3/\tau_{\sigma l}^{(2)}. \qquad (D3c)$$

where the subindex $l$ denoting a physical mechanism has been omitted for simplicity.
Substituting the stress-strain relations (D1a-c) in the equation of motion (12) and making use of the strain-displacement relations

$$S_1 = \frac{\partial u_x}{\partial x}, \quad S_3 = \frac{\partial u_z}{\partial z}, \quad S_5 = \frac{\partial u_x}{\partial z} + \frac{\partial u_z}{\partial x}, \qquad (D4)$$

together with equations (D3a-c), defines an equation of the type (23) whose unknown variable and body force vectors, and spatial operator are given by equations (27), (28) and (29) respectively.

## REFERENCES

Carcione, J.M., Kosloff, D., & Kosloff, R., 1988c. Wave propagation simulation in a linear viscoelastic medium, Geophys. J. Roy. Astr. Soc., **95**, 597-611.

# APPENDIX E

## SIMULATED WAVEFIELDS IN HOMOGENEOUS SANDSTONE

This appendix present the results of wave propagation in sandstone for the rheologies indicated in Table 1.

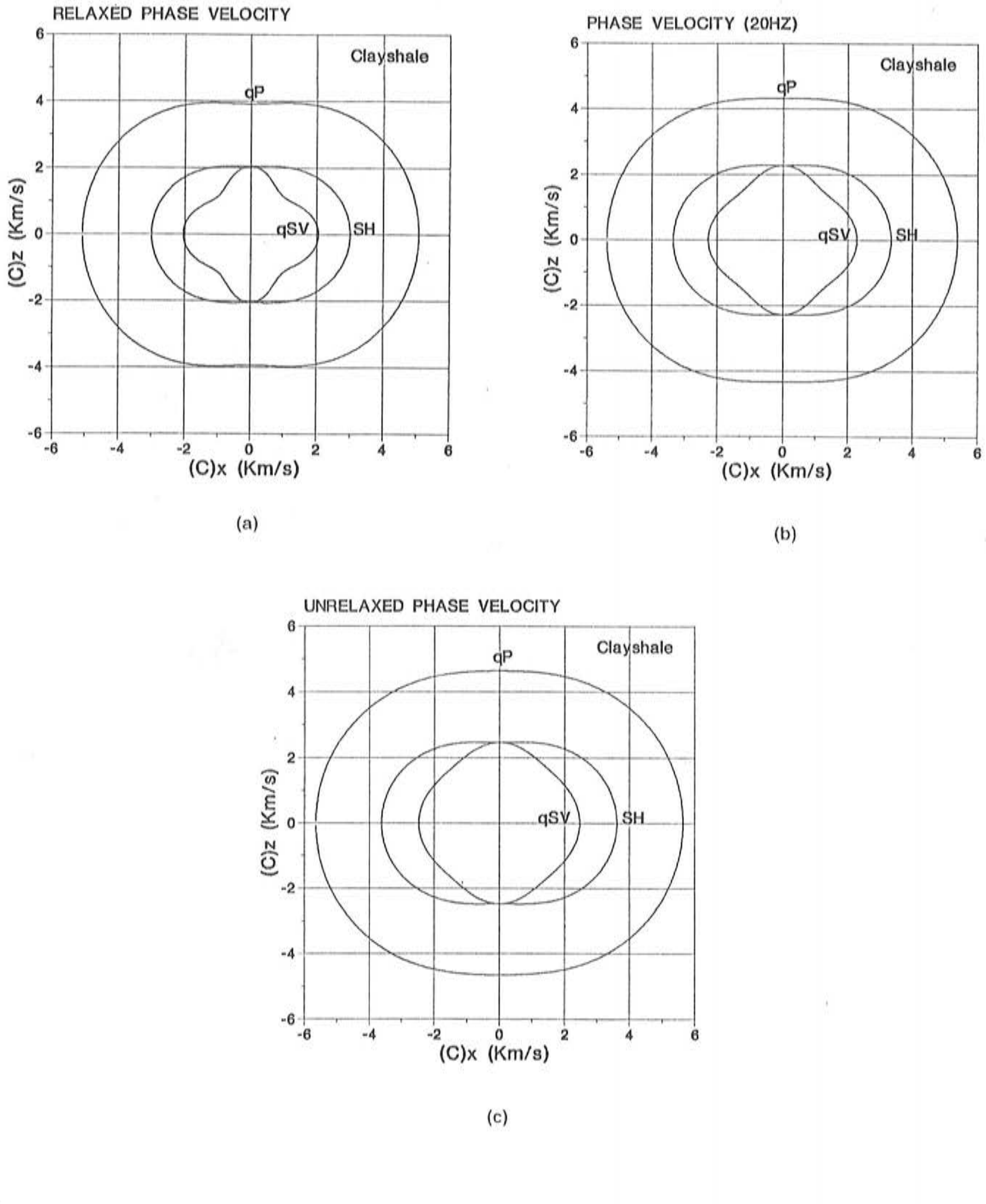


**Figure B1.** Phase velocity curves for TIV clayshale. Propagation in the $(x,z)$-plane, (a) relaxed, (b) $f = 20Hz$, (c) unrelaxed.

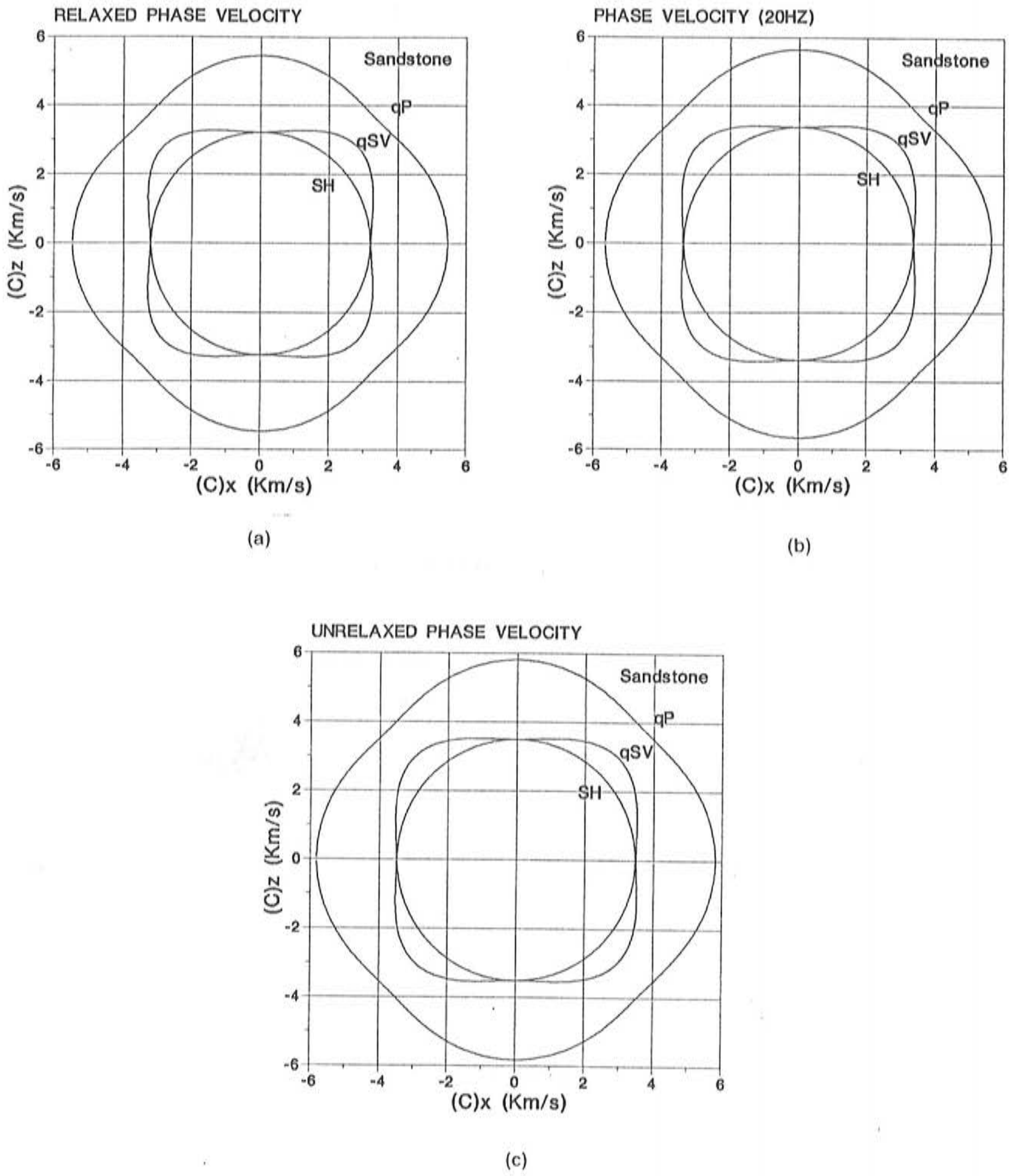


**Figure B2.** Phase velocity curves for TIV sandstone. Propagation in the $(x,z)$-plane, (a) relaxed, (b) $f = 20Hz$, (c) unrelaxed.

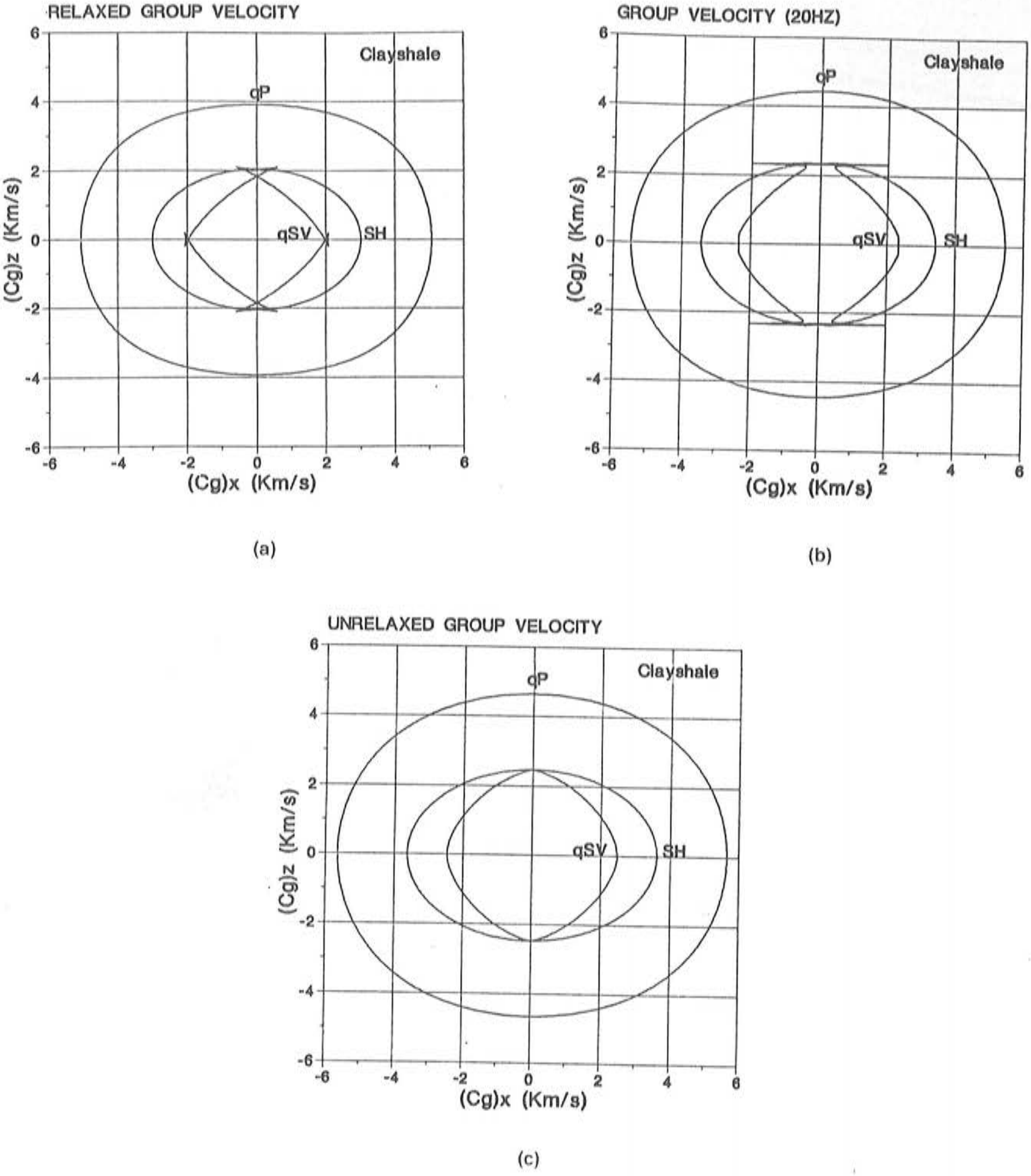


**Figure B3.** Group velocity curves for TIV clayshale. Propagation in the $(x,z)$-plane, (a) relaxed, (b) $f = 20Hz$, (c) unrelaxed.

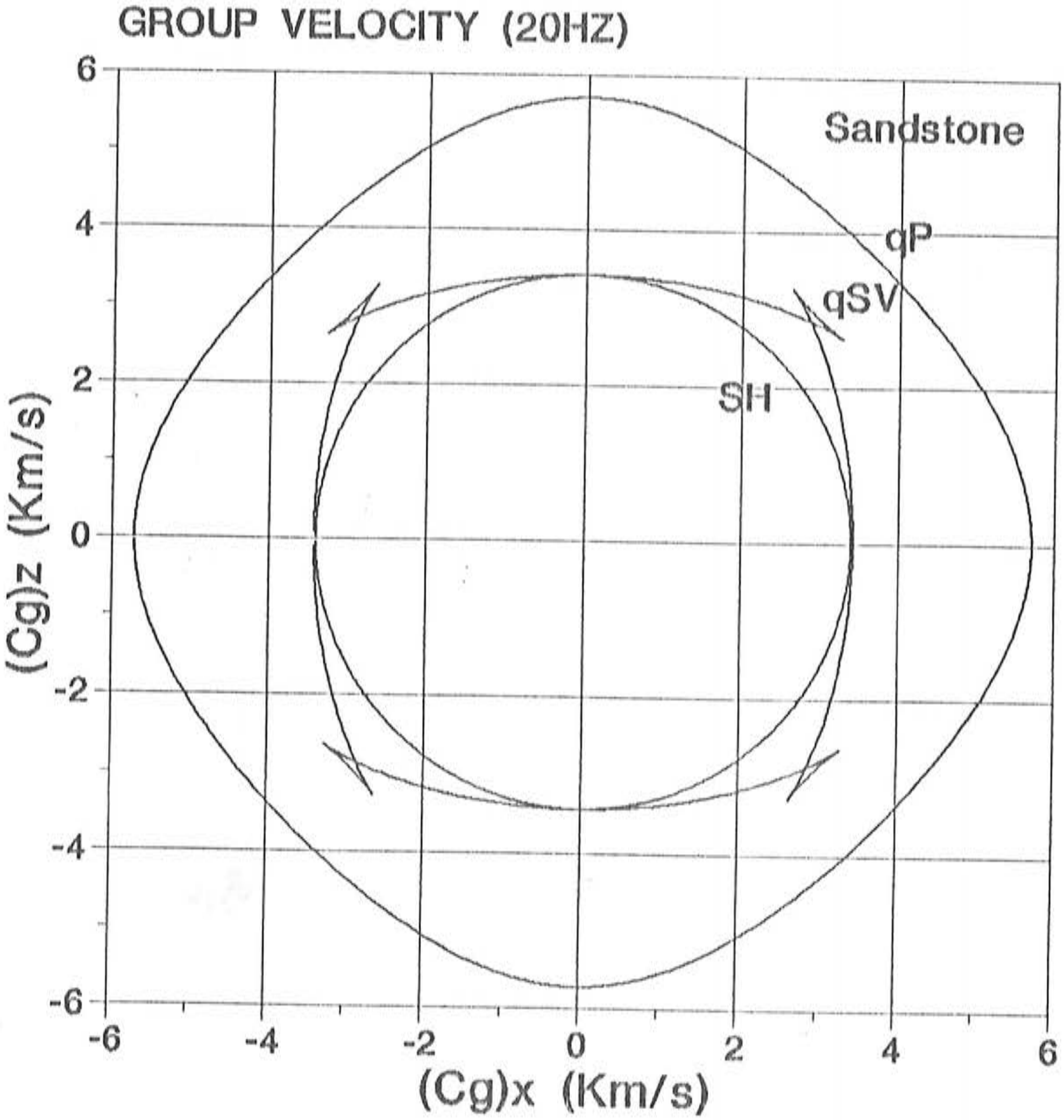


**Figure B4.** Group velocity curves for TIV sandstone. Propagation in the $(x,z)$-plane, $f = 20Hz$.

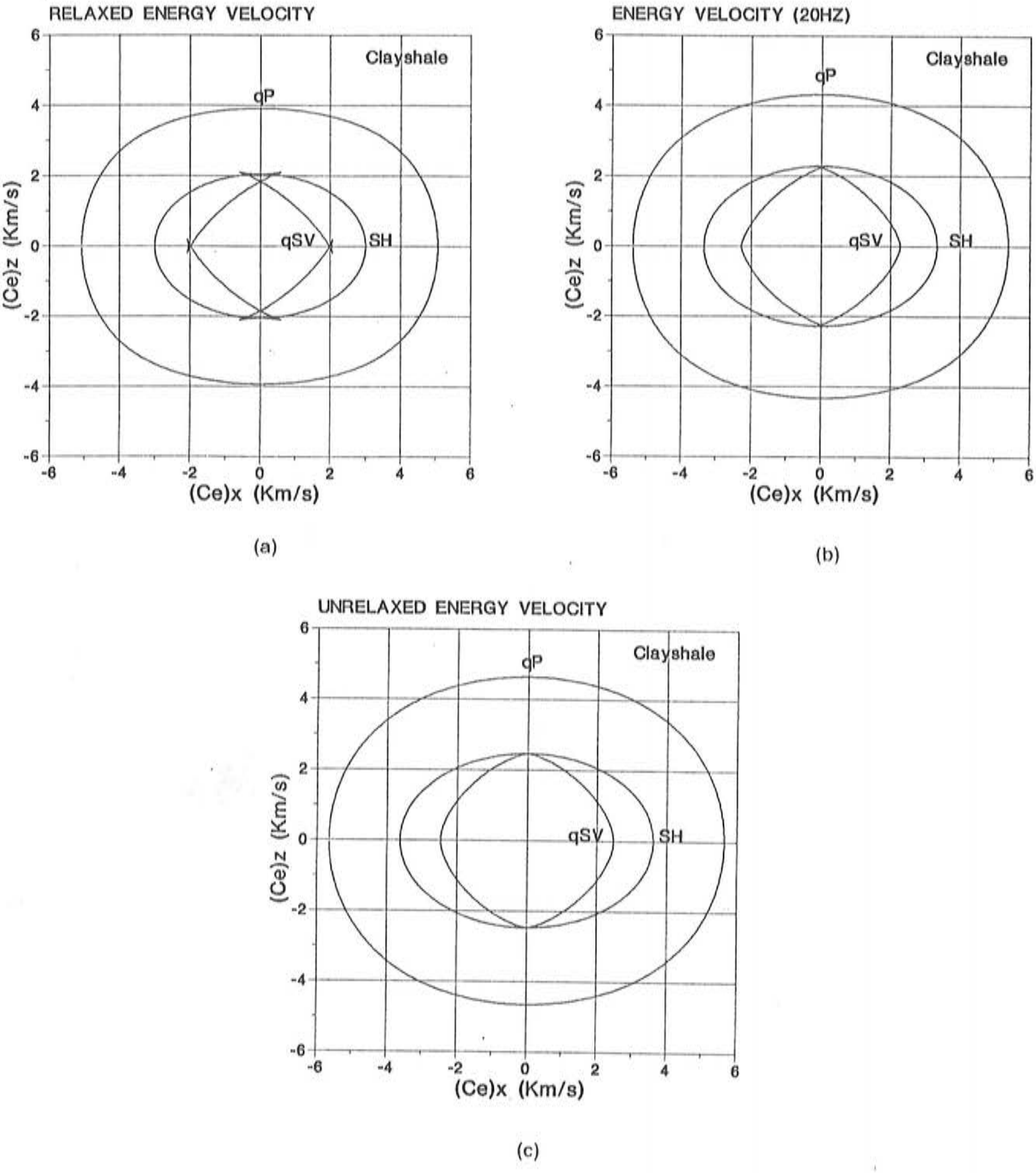


**Figure B5.** Energy velocity curves (wavefronts) for TIV clayshale. Propagation in the $(x,z)$-plane, (a) relaxed, (b) $f = 20Hz$, (c) unrelaxed.

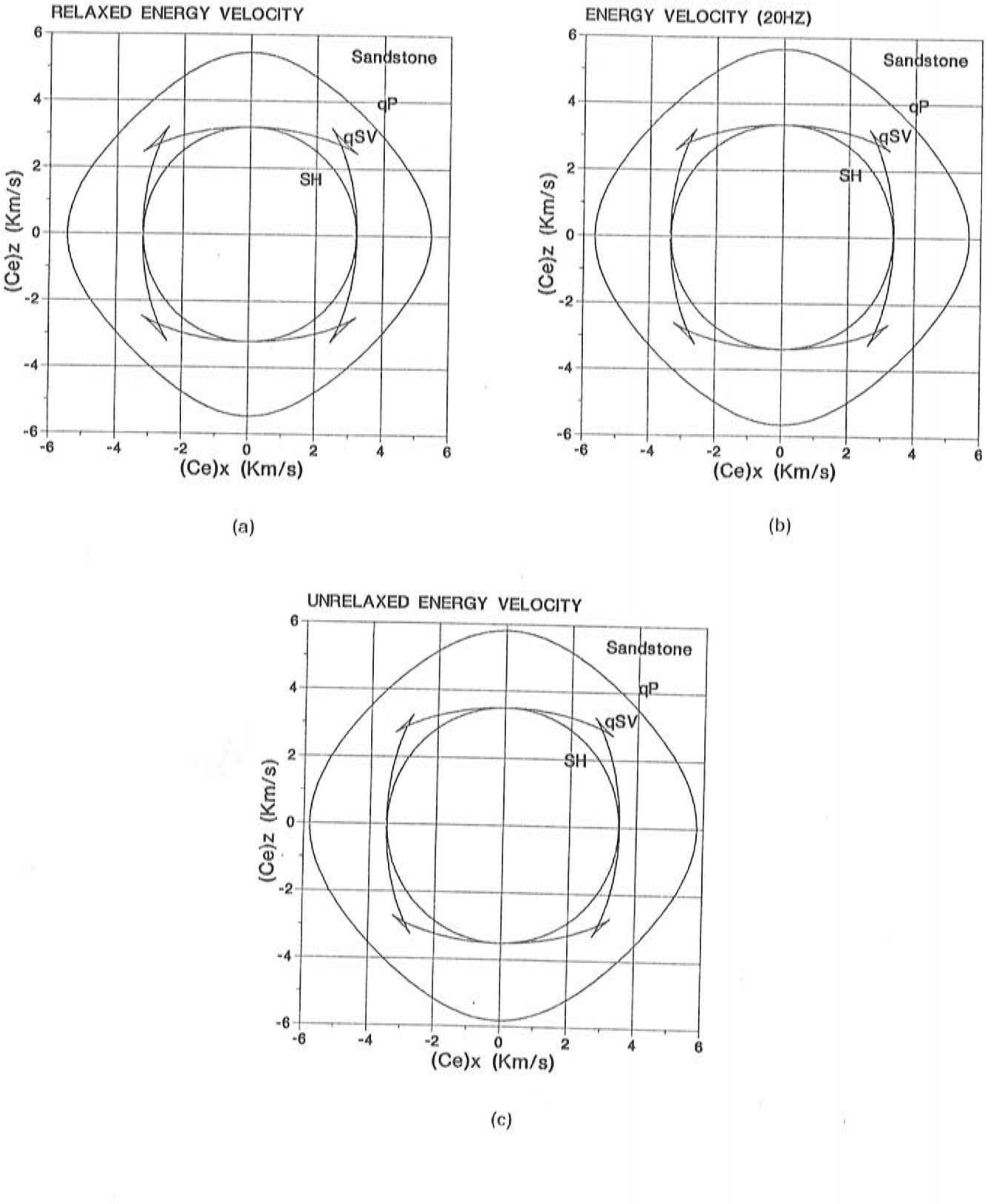


**Figure B6.** Energy velocity curves (wavefronts) for TIV sandstone. Propagation in the $(x,z)$-plane, (a) relaxed, (b) $f = 20Hz$, (c) unrelaxed.

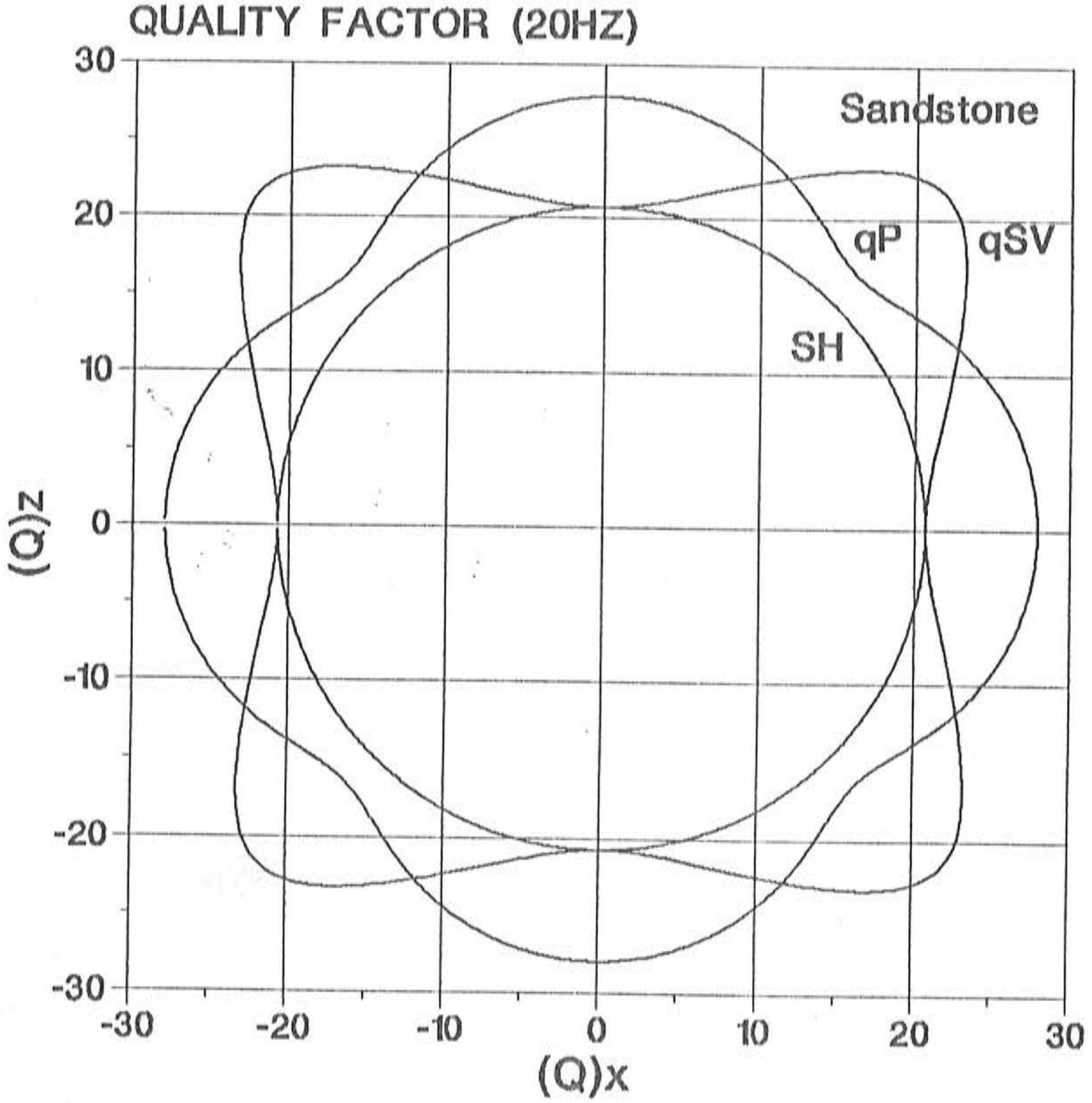


**Figure B7.** Quality factor curves for TIV clayshale at $f = 20Hz$ Propagation in the $(x,z)$-plane. The curves are polar representations of the form $Q_x = Ql_x$, $Q_z = Ql_z$, valid for homogeneous waves for which the attenuation and propagation directions coincide.

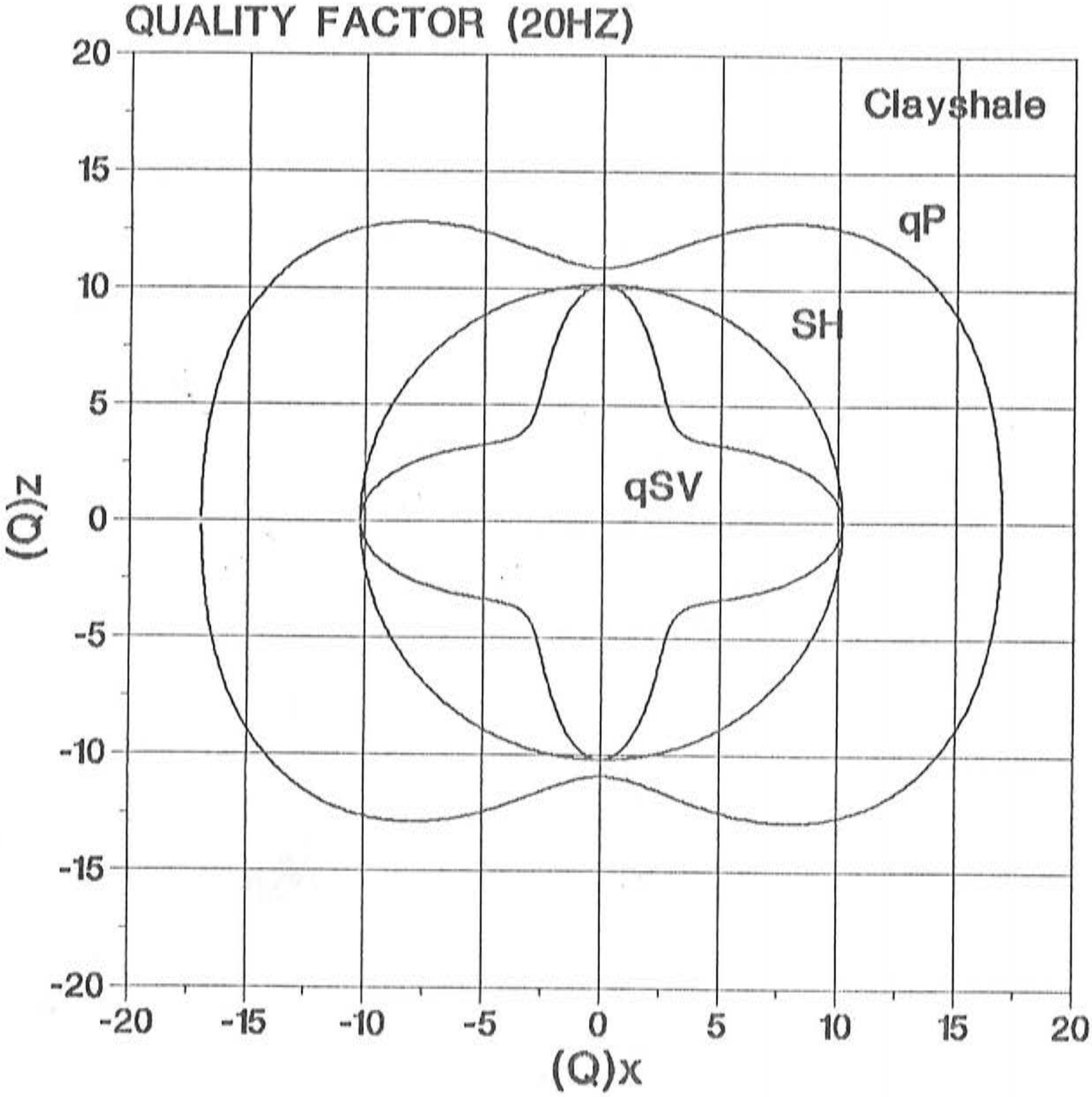


**Figure B8.** Quality factor curves for TIV sandstone at $f = 20Hz$ Propagation in the $(x,z)$-plane. The curves are polar representations of the form $Q_x = Ql_x$, $Q_z = Ql_z$, valid for homogeneous waves for which the attenuation and propagation directions coincide.

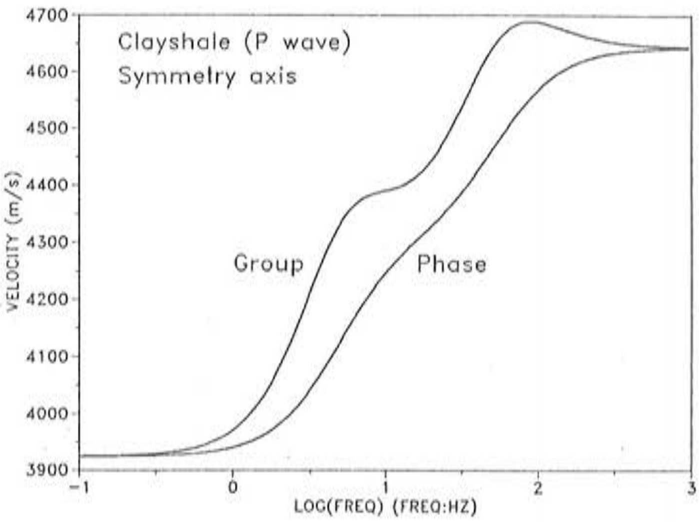


(a)

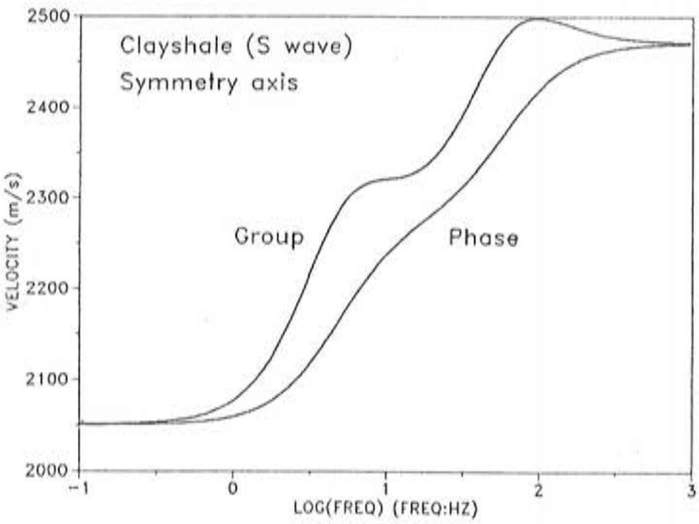


(b)

**Figure B9.** Phase and group velocities versus frequency for TIV clayshale in the symmetry axis , (a) $P$ wave, (b) $S$ wave.

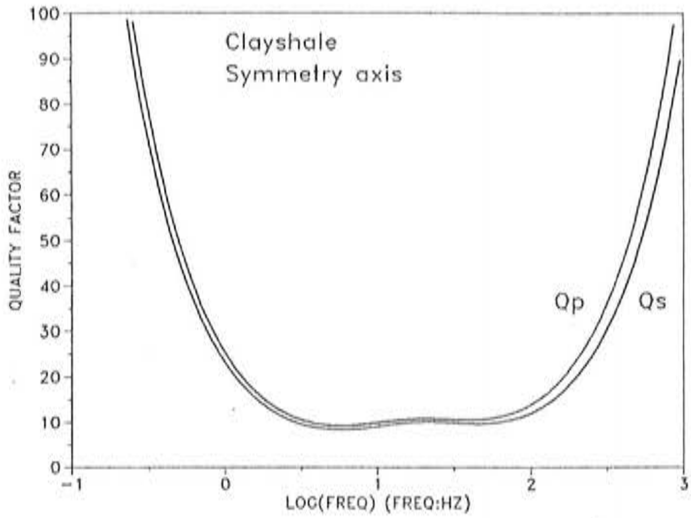


(a)

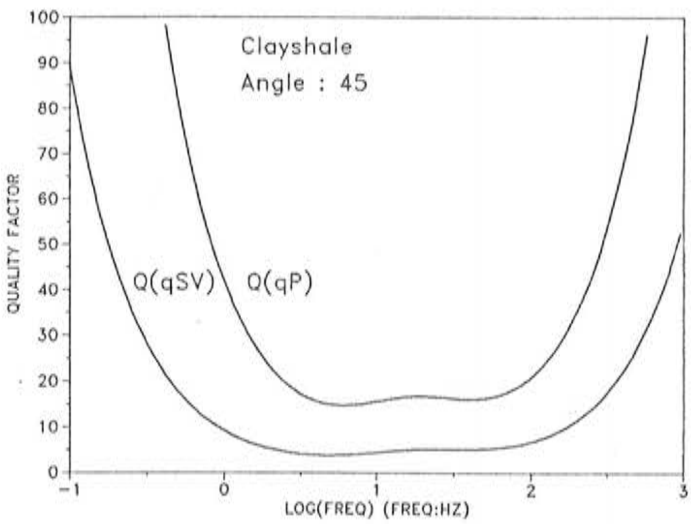


(b)

**Figure B10.** Quasi-longitudinal and quasi-transverse quality factors versus frequency for TIV clayshale, (a) symmetry axis, (b) $\theta = \pi/4$.

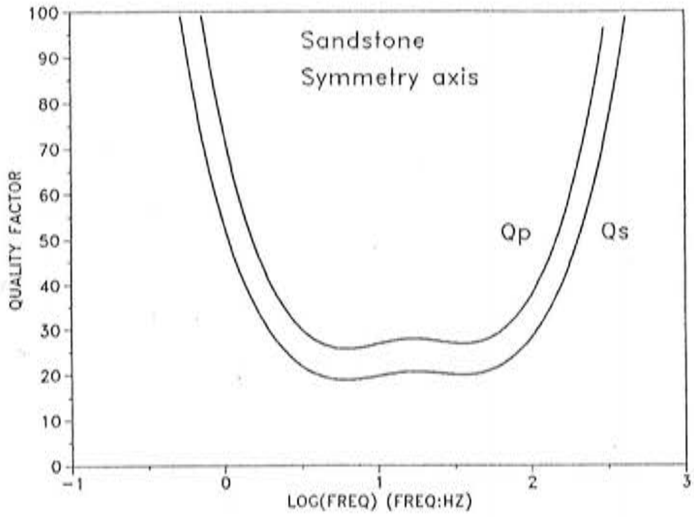


(a)

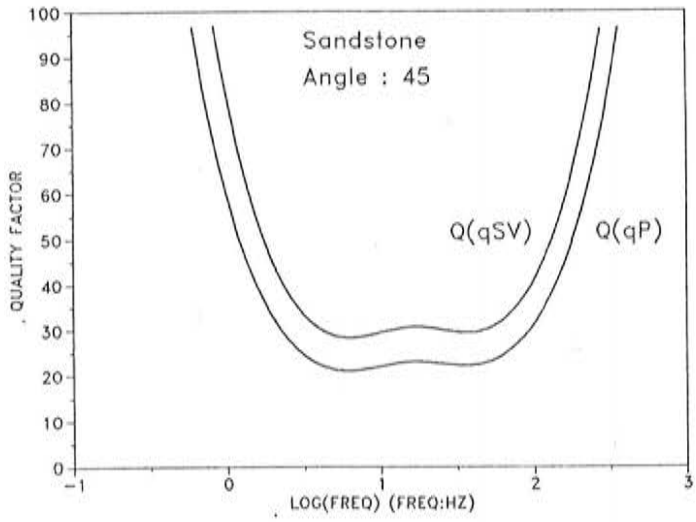


(b)

**Figure B11.** Quasi-longitudinal and quasi-transverse quality factors versus frequency for TIV sandstone, (a) symmetry axis, (b) $\theta = \pi/4$.

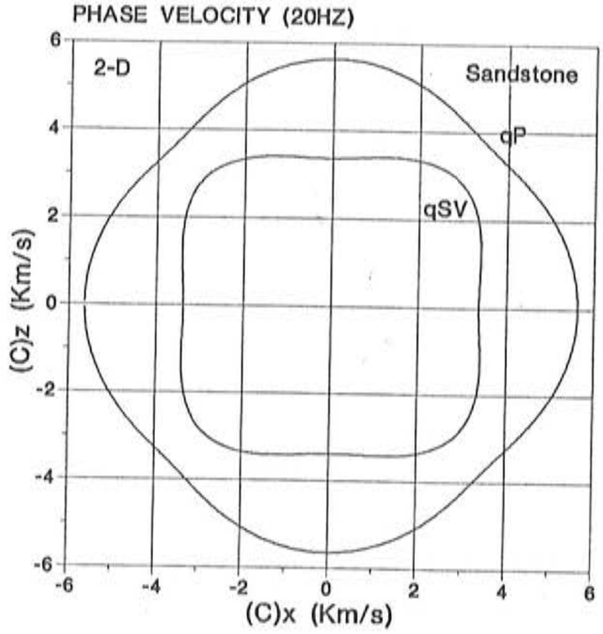


(a)

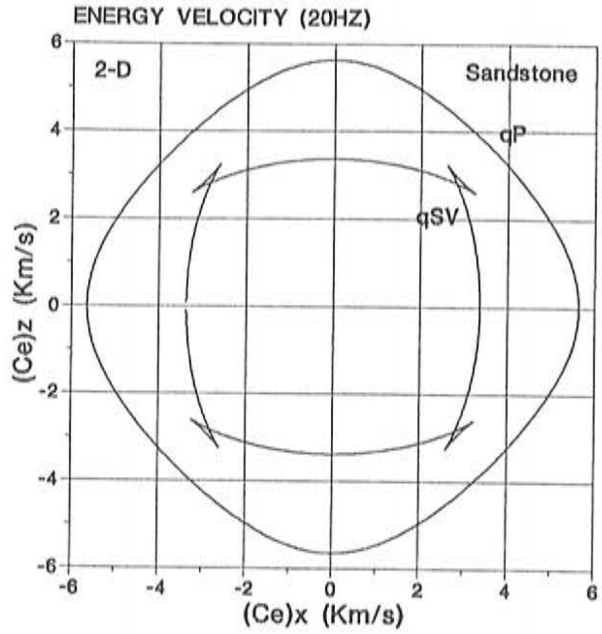


(b)

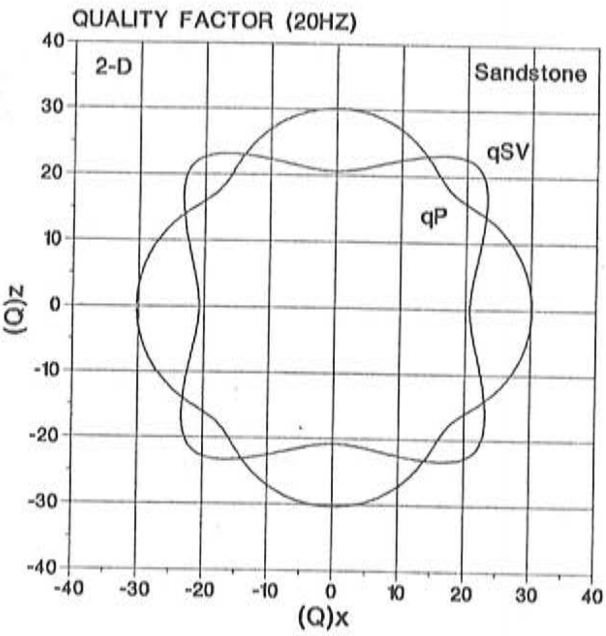


(c)

**Figure E1.** 2-D TIV sandstone, (a) phase velocity curves, (b) energy velocity curves (wavefronts), (c) quality factor curves. Frequency is 20 Hz.

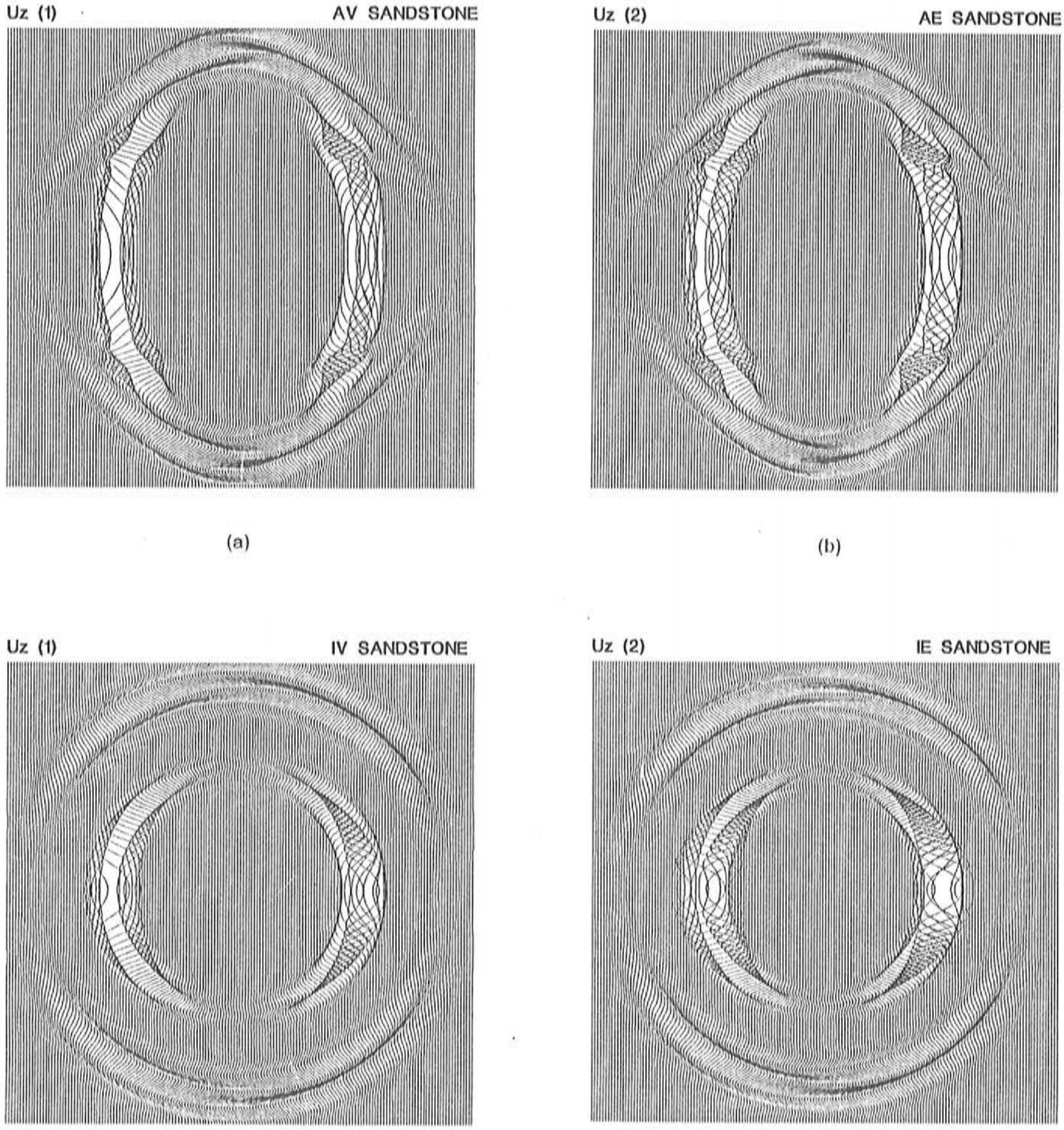


**Figure E3.** $u_z$ -component of the wavefield at $t = 0.32s$ for sandstone, (a) AV rheology, (b) AE rheology, (c) IV rheology, (d) IE rheology. The numerical mesh is 165 x 165 size, with a grid spacing $DX = DZ = 20m$. The motion is initiated by a vertical source whose time history is given by equation (31). The number between parenthesis denotes the plotting scale. The elastic amplitudes are reduced a factor 2 relative to the viscoelastic amplitudes.

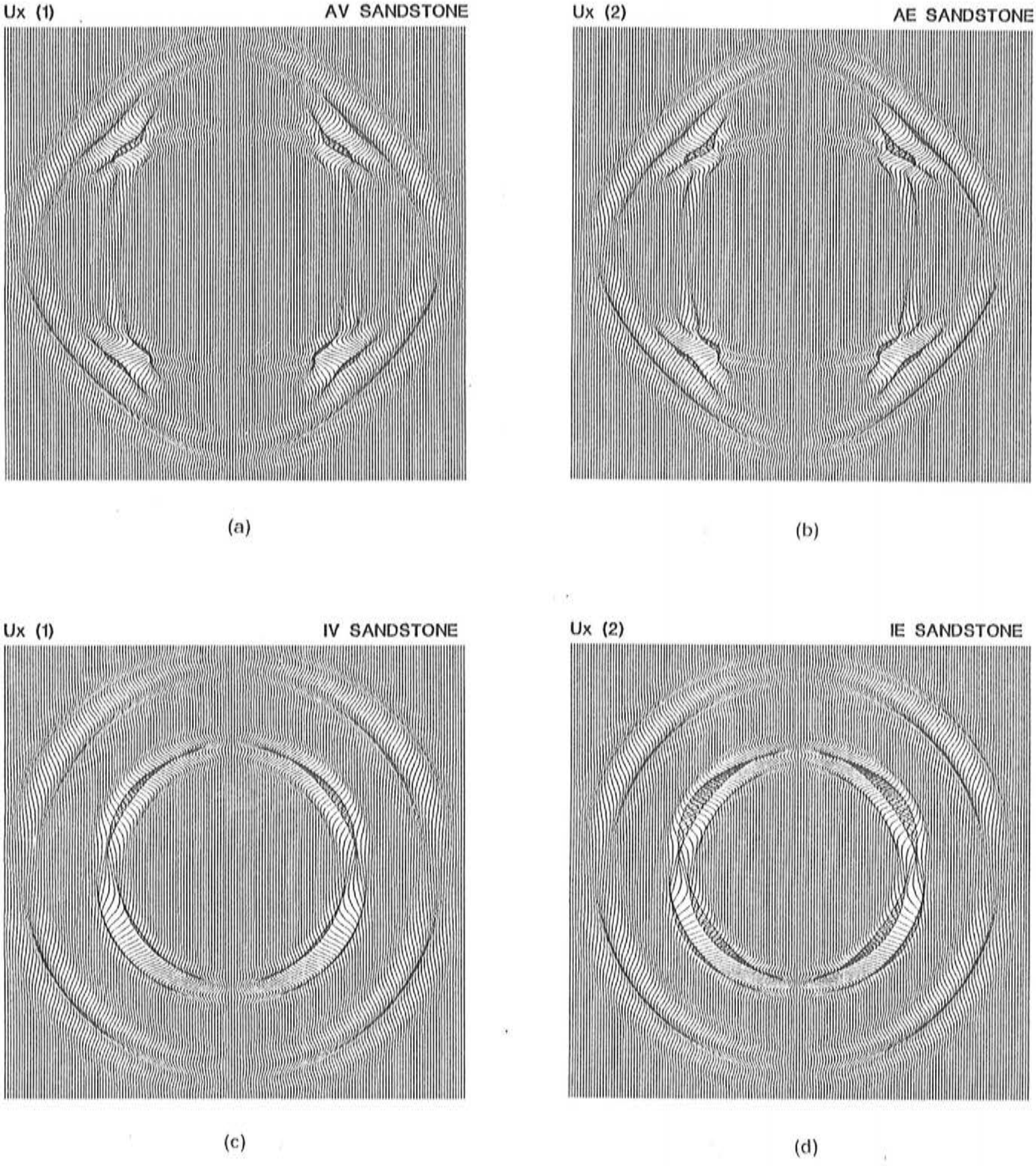


**Figure E2.** $u_x$ -component of the wavefield at $t = 0.32s$ for sandstone, (a) AV rheology, (b) AE rheology, (c) IV rheology, (d) IE rheology. The numerical mesh is 165 x 165 size, with a grid spacing $DX = DZ = 20m$. The motion is initiated by a vertical source whose time history is given by equation (31). The number between parenthesis denotes the plotting scale. The elastic amplitudes are reduced a factor 2 relative to the viscoelastic amplitudes.